The LisbOn KInetics Boltzmann solver

A. Tejero-del-Caz[1], V. Guerra[1], D. Gonçalves[1], M. Lino da Silva[1], L. Marques[2], N. Pinhão[1], C. D. Pintassilgo[1,3], L. L. Alves[1]

[1] Instituto de Plasmas e Fusão Nuclear, Instituto Superior Técnico, Universidade de Lisboa, Av. Rovisco Pais, 1049-001 Lisboa, Portugal

[2] Centro de Física das Universidades do Minho e do Porto, Campus de Gualtar, Braga, Portugal

[3] Faculdade de Engenharia da Universidade do Porto, Porto, Portugal

E-mail: `llalves@tecnico.ulisboa.pt`

January 29, 2019

Abstract. The LisbOn KInetics Boltzmann (LoKI-B) is an open-source simulation tool (`https://github.com/IST-Lisbon/LoKI`) that solves a time and space independent form of the two-term electron Boltzmann equation, for non-magnetised non-equilibrium low-temperature plasmas excited by DC/HF electric fields from different gases or gas mixtures. LoKI-B was developed as a response to the need of having an electron Boltzmann solver easily addressing the simulation of the electron kinetics in any complex gas mixture (of atomic / molecular species), describing first and second-kind electron collisions with any target state (electronic, vibrational and rotational), characterized by any user-prescribed population. LoKI-B includes electron-electron collisions, it handles rotational collisions adopting either a discrete formulation or a more convenient continuous approximation, and it accounts for variations in the number of electrons due to non-conservative events by assuming growth models for the electron density. On input, LoKI-B defines the operating work conditions, the distribution of populations for the electronic, vibrational and rotational levels of the atomic / molecular gases considered, and the relevant sets of electron-scattering cross sections obtained from the open-access website LXCat (`http://www.lxcat.net/`). On output, it yields the isotropic and the anisotropic parts of the electron distribution function (the former usually termed the *electron energy distribution function*), the electron swarm parameters, and the electron power absorbed from the electric field and transferred to the different collisional channels. LoKI-B is developed with flexible and upgradable object-oriented programming under MATLAB®, to benefit from its matrix-based architecture, adopting an ontology that privileges the separation between tool and data. This topical review presents LoKI-B and gives examples of results obtained for different model and real gases, verifying the tool against analytical solutions, benchmarking it against numerical calculations, and validating the output by comparison with available measurements of swarm parameters.

Accepted for publication in *Plasma Sources Sci. Technol.* (2019)

1. Introduction

Low-temperature plasmas (LTPs) are highly-energetic highly-reactive environments, exhibiting a low density of charged particles (ionisation degrees $\sim 10^{-6} - 10^{-3}$), high electron temperature (~ 1 eV) and variable heavy-species characteristic temperatures, ranging from 300 K to $\sim 10^4$ K. These features open the way to develop plasma-based technologies that use different energy distribution scenarios, through efficient channeling of the energy to targeted species, both in volume and in plasma-facing substrates. Electrons are key in this strategy, as they convey the energy available to the heavy species through various collisional channels that stimulate the reactivity of the plasma. Therefore, it becomes paramount to control the energy distribution of the electrons, tailoring it as to fine-tune the energy transferred to the heavy species. Detailed knowledge of the electron energy distribution is essential also to obtain quantitative information for use in fluid / global predictive models or in the analysis of experimental diagnostics, by calculating quantities such as rate coefficients, transport parameters and fractional average powers, hereafter termed electron macroscopic parameters.

The electron kinetics can be described in detail by solving numerically the electron Boltzmann equation (EBE) for LTPs [1], usually written under an approximation framework that expands the electron distribution function in powers of some quantity around the equilibrium, assuming that the thermal velocities are larger than the drift velocities resulting from the combined anisotropic effects of electromagnetic applied forces and pressure gradients. The problem has been solved throughout the years by many different research groups around the world, that developed EBE solvers as standalone codes or as routines embedded into other numerical models. We would like to highlight the pioneering contributions of some authors [2], to whom the community is grateful for advancing knowledge on topics related to the electron kinetics: gas discharges in molecular nitrogen and hydrogen were extensively investigated in the early works of Frost and PheIps [3], Engelhardt and Phelps [4], Newman and Detemple [5] and Taniguchi *et al* [6]; Nighan included an EBE solver in a global model for $N_2/CO_2/CO$ gas-discharge lasers [7]; Morgan [8] and Rockwood [9] presented the details of a computer code for solving the EBE in a low-pressure positive column, and later Rockwood *et al* [10, 11] and Winkler [12] used this approach to study Hg, Ar/Hg, $CO_2/N_2/He$ and CO/N_2 gas discharges; Elliott and Greene [13] and Bretagne *et al* [14] analysed electron-beam-generated xenon and argon plasmas; Capitelli *et al* [15,16], and later Loureiro and Ferreira [17], solved the EBE coupled to rate balance equations describing the vibrational kinetics of several gases (the first contributions being for HCl and N_2); Pitchford, Phelps *et al* carried out a systematic study of the effects of various simplifying approximations on the solutions of the EBE in molecular gases, such as N_2, describing techniques for adding higher-degree spherical harmonics to the two-term approximation [18], analysing the errors introduced by the two-term approximation in the calculation of excitation rate coefficients at various applied electric fields [19], and examining the effects of various approximations to the distribution in energy of secondary electrons produced in

electron-impact ionizations [20]; the time relaxation of the EEDF was firstly analysed by Capitelli, Gorse, Winkler *et al* [21–24]; Morgan and Penetrante released "ELENDIF: A time-dependent Boltzmann solver for partially ionized plasmas" [25], distributing a compiled version of this code upon payment of a fee.

With the arrival of the internet era, various authors have accepted to share the simulation tools developed, for the benefit of the LTP community. Examples of these tools are ELENDIF [25, 26], BOLSIG+ [27, 28], EEDF [29], BOLOS [30], METHES [31, 32], Magboltz [33, 34] and MultiBolt [35, 36], the latter four being open-source tools. BOLOS is a Python library using an algorithm similar to that adopted in BOLSIG+, METHES is a Monte Carlo collision code written in MATLAB® [37] for the simulation of electron transport in LTPs, and MultiBolt is a multi-term Boltzmann equation solver, also written in MATLAB®, to benchmark cross-section sets with interest for LTP models. BOLSIG+, BOLOS, METHES and MultiBolt accept input files with electron scattering cross sections obtained from the LXCat open-access website [38]. Magboltz is a Fortran code with hardcoded data that combines a multi-term expansion (to the third order) of the electron distribution function with a Monte Carlo integration technique for solving the EBE, to ensure calculation accuracies below 1% for the Lorentz angle. All other tools mentioned here solve the EBE under the classical two-term approximation [39, 40]. Magboltz and BOLSIG+ describe the drift and diffusion of electrons in a LTP under the influence of electric and magnetic fields at any angle with each other, whereas EEDF can consider crossed electric and magnetic fields only. BOLSIG+ and EEDF accept also high-frequency (HF) excitation electric fields as input data. MultiBolt includes a multi-harmonic model for intense microwave and terahertz excited LTPs [41]. All other codes mentioned here are for LTPs excited by a stationary (DC) electric field.

Most of these codes take into account the variation of the electron density due to non-conservative electron scattering mechanisms, such as ionisation, attachment and recombination. The Monte-Carlo codes, BOLSIG+ and MultiBolt further calculate transverse and longitudinal bulk / flux swarm parameters, by adopting a density gradient expansion, and they also allow for an electron density growth under Steady-State Townsend (SST) or Pulsed Townsend (PT) conditions, by prescribing the energy sharing between the primary and the secondary electrons resulting from ionisation events (METHES), or by taking the limiting cases of no-sharing and/or equal-energy-sharing (BOLSIG+ and MultiBolt). In principle, all these codes can solve the EBE for a mixture of gases chosen by the user, taking into account electron collisions of first and second kind with electronic-like excited levels, but this feature is not available (or is difficult to extend) to the subset of vibrational levels within an electronic level and the subset of rotational levels within a vibrational level.

It is unquestionable that substantial progresses were made in setting the basic model formulations and computational techniques describing LTPs. However, maintaining this route requires a community-wide change in its mode of operation, by borrowing best practices from other disciplines. A closer linking between theory and computation,

the adoption of high performance and cloud computing (HPCC) techniques, the implementation of verification & validation (V&V) standards, the distribution of open-source codes, and the support of open-access databases are examples of these practices [42]. The codes previously mentioned implement some of these best practices, because they use an open-access database, or because they are open-source tools, or both in a few cases.

The concern about the correctness of computer simulations is not new, and the pioneering efforts of several authors to introduce V&V strategies in the development of codes is to be recognized. These strategies concern both the definition of test problems to be used in verification procedures [43–46], and the swarm validation of codes and cross section data [47]. The latter research programme relates to the highly-sensitive procedure for obtaining cross sections from electron transport coefficients, which is discussed with detail in several publications [48–54].

Recently, there has been a growing awareness of the community about the relevance of defining and implementing structured V&V approaches, to be routinely followed as part of code development [55]. This attitude is motivating collaborative efforts for discussing V&V standards [56], in a network approach where the needs of the community are necessarily considered. On this latter point, when the focus is on the description of the electron kinetics, there is obvious demand for predictive tools providing an adequate and user-friendly handling of the energy transfer to / from the internal degrees of freedom of atoms and molecules (namely in what refers the electron-impact excitation / de-excitation of electronic, vibrational and rotational levels), in order to obtain quality information that can be used as input data in macroscopic models or in the analysis of experimental diagnostics.

This work presents the open-source simulation tool LisbOn KInetics Boltzmann (LoKI-B), that solves a time and space independent form of the two-term EBE for non-magnetised LTPs excited by DC/HF electric fields, including first-kind, second-kind and electron-electron collisions, and assuming either a space-homogeneous exponential temporal growth or a time-constant exponential spatial growth of the electron density, as simplifying conditions to account for changes in the number of electrons due to non-conservative events (e.g. the production of secondary electrons born in ionisation events). Rotational collisions can be described using either a discrete formulation or a more convenient continuous approximation [57], which was formulated and tested for homonuclear diatomic molecules. On output, LoKI-B gives the electron distribution function and the various electron macroscopic parameters, namely swarm parameters and power balance terms, calculated using either the distribution function obtained from the solution to the EBE or some other form prescribed by the user. The electron macroscopic parameters are relevant for the adjustment of electron-scattering cross sections, the analysis of the distribution of power among the collisional channels, and the control upon calculation errors and validity limits. LoKI-B leverages on the scientific heritage in the field of nonequilibrium plasma kinetics of the Portuguese group N-Plasmas Reactive: Modeling and Engineering (N-PRiME) [58], and it was developed

under the framework of a dedicated project [59], resorting to well-grounded scientific foundations established years ago [60, 61]. LoKI-B is a flexible and upgradable tool developed with object-oriented programming under MATLAB® [37], to benefit from its matrix-based architecture. The code adopts an ontology that privileges the separation between tools and data, namely by using a well-defined interface and data format.

The organisation of the paper is the following. Section 2 presents arguments to motivate users for using LoKI-B. Section 3 recalls the basics of the EBE, reviewing its two-term formulation (focusing on the ionisation collision operator and the definition of the effective/total electron-neutral momentum-transfer cross section), showing the flexibility in defining the electron excitation conditions from the input data available, providing minimal details about the numerical solution, and presenting the main electron macroscopic parameters calculated as output. Section 4 gives examples of results obtained with LoKI-B for different model and real gases, putting forward the main features and the flexibility of operation of the simulation tool, verifying it against analytical results, benchmarking it against numerical calculations obtained with BOLSIG+, and validating the output by comparison with available measurements of swarm parameters. Section 5 presents some final remarks and future guidelines.

2. Why using LoKI-B ?

LoKI-B was developed as a response to the need of having an electron Boltzmann solver easily addressing the simulation of the electron kinetics in complex gas mixtures. To our knowledge, this requirement is not fully met by none of the solvers available for public use, including BOLSIG+, undoubtedly the one most adopted by the LTP community. As mentioned before, BOLSIG+ (version 12/2017 beta [28]) features several physical models that allow its use in many different working conditions, namely: electron drift and diffusion under the influence of electric and magnetic fields at any angle with each other; density-gradient expansion allowing calculating the transverse and longitudinal bulk / flux swarm parameters; influence of electron-electron collisions on the first anisotropy; HF excitation; PT and SST electron density growth due to non-conservative electron scattering mechanisms. The inclusion of stepwise-inelastic and superelastic collisions is also announced through the selection of the option "Superelastics". However, this option activates these mechanisms for *all* the target states considered in the simulations, assuming fractional populations for the upper and lower states of each transition calculated from bi-Maxwellian Boltzmann factors, with a transition from the gas temperature T_g to an excitation temperature $T_{\rm exc}$ occurring around an energy $U_{\rm tr}$ (T_g, $T_{\rm exc}$ and $U_{\rm tr}$ are provided by the user). Moreover, this feature does not allow discriminating the nature of the different states considered, treating electronic and vibrational states in a similar way (by using electron-scattering cross sections labelled as `EXCITATION`, to describe *both* electronic and vibrational transitions), with populations that are normalized separately in pairs, for each excitation process. The populations of rotational states are normalized in a more rigorous way, over its ensemble, always

with the restriction of using a bi-Maxwellian Boltzmann distribution. As an alternative solution to the previous limitations, BOLSIG+'s users can trigger stepwise-inelastic and superelastic mechanisms by using a double-arrow ($<->$) when defining each electron-collision mechanism in the cross-section input file. In principle, this procedure allows a free choice of the populations for each target state, and of the normalization rules to be satisfied by each ensemble of states (electronic, vibrational, rotational). However, in this case BOLSIG+ treats the various target states as individual components of a gas mixture, for each of which "mole fractions" must be provided, introducing additional complications. In particular, BOLSIG+ adopts the standard format of LXCat for the cross-section input files, where each target corresponds simply to a "gas", with no details on its quantum configuration. This way, there is no discrimination between an electronic ground/excited-state and a vibrational ground/excited-state (within the former), unless the user splits the input file of the "gas", creating as many files as the target states to be considered, in order for BOLSIG+ to import them as "pseudo-gas-components" of a mixture. Naturally, each one of these files should contain not only the excitation cross sections for the corresponding target, but also its elastic momentum-transfer cross section, which can be difficult to deduce if the original data in the "gas" input file is for the effective momentum-transfer cross section (see the discussion in section 3.2).

Compared to BOLSIG+, the current version of LoKI-B is more limited in the features of some physical models (only non-magnetized plasmas are described; no density-gradient expansion is included; the impact of electron-electron conditions in the first anisotropy is not considered), but in other cases it includes further options (e.g. the rotational excitation / deexcitation of homonuclear diatomic molecules can be described using a convenient continuous approximation CAR, see section 3.1; the sharing of energy between the two electrons involved in ionization events can be more generally described by a differential cross section, in addition to the limiting cases of no-sharing or equal-energy-sharing, see section 3.2; the electron macroscopic parameters can be calculated adopting a generalised Maxwellian distribution function, or any other function prescribed by the user, see section 3.5). Principally, LoKI-B was designed for the simulation of the electron kinetics in *any* complex gas mixture (of atomic / molecular species), describing first and second-kind electron collisions with *any* target state (electronic, vibrational and rotational), characterized by *any* user-prescribed population, easily defined through a formula or a text file (e.g. a Boltzmann distribution at gas temperature for the rotational states; a Treanor-Gordiets distribution at given excitation temperature for the vibrational states; and a set of self-consistently-calculated or measured populations for the electronic states, see examples in section 4). Thus, in LoKI-B, the structure of each target state must be detailed according to the standard rules of atomic and molecular physics, and the limitations previously reported for BOLSIG+ in the handling of input data from LXCat are solved by including extra specifications in the input files (see section 3.3). Naturally, this flexibility is enhanced by the open-source nature of LoKI-B, making the code transparent and easy to use, and although these features are of more technical nature they are perceived today as

compelling advantages for the users [62].

3. The electron Boltzmann equation

The simulation tool LoKI-B solves a time and space independent form of the two-term EBE, calculating the electron energy distribution function (EEDF) and the corresponding electron macroscopic parameters. The current version of the tool is for non-magnetised LTPs. The scientific foundations of LoKI-B were established years ago [60, 61], and are based on the early works of Lorentz, Holstein, Allis and Delcroix [39, 40, 63, 64]. A recent topical review [1], integrated in the collection *Foundations of low-temperature plasmas and their applications* published by *Plasma Sources Science and Technology*, gives a summary of the essentials of the EBE, when written for an electron distribution function expanded in Legendre polynomials $P_l(\cos\theta)$ around the angle θ, defining the spatial orientation of the velocity vector with respect to the polar direction of the total anisotropy (produced by electric fields and density gradients).

3.1. General formulation

LoKI-B describes the electron kinetics of a plasma with electron density n_e, excited from a general mixture of atomic / molecular gases, by applying an electric field along the z-axis with the form

$$\vec{E}(t) = -E_p \cos(\omega t)\, \vec{e}_z \quad , \tag{1}$$

where the oscillation frequency ω is either set to zero (in the DC case) or taken much larger than the typical collision frequency ν_c (in the HF case). Each gas k of the mixture has mass M_k and particle density N_k, such that the total gas density is $N = p/(k_B T_g) \equiv \sum_k N_k$, with p the total gas pressure and T_g the gas temperature (k_B is the Boltzmann constant), assumed equal for all k-gas components. Moreover, each gas k is composed by several electronic levels k_i with particle density N_{k_i}, such that the k-gas density is $N_k \equiv \sum_i N_{k_i}$. We also introduce the following normalised densities: the *gas fraction* in the mixture $\chi_k \equiv N_k/N$; the *population* of level k_i, relative to the k-gas density, $\xi_{k_i} \equiv N_{k_i}/N_k$; and the *reduced density* of level k_i, relative to the total gas density, $\delta_{k_i} \equiv N_{k_i}/N$, such that $\delta_{k_i} = \xi_{k_i}\chi_k$. Note that each k_i-level can include several vibrational sub-levels k_{i_v}, each one composed by several rotational sub-levels $k_{i_{v_J}}$. The definition of the normalised densities for each one of these sub-levels follows the same ontology as for the k_i levels, and therefore can be obtained by a straightforward generalisation of ξ_{k_i} and δ_{k_i}.

In the classical two-term approximation, the electron distribution function can be written assuming a separation between the Legendre expansion of the energy distribution and the space-time profile of the electron density $n_e(z,t)$ as follows

$$F(z,u,t) \simeq \left\{ f^0(u) + \left[\vec{f}^1(u) \cdot \frac{\vec{v}}{v} \right] \cos\omega t \right\} n_e(z,t)$$

$$= \left[f^0(u) + f^1(u)\cos\theta\cos\omega t\right] n_e(z,t) \quad , \tag{2}$$

where $u = m_e v^2/(2e)$ is the electron kinetic energy in eV (with m_e and e the electron mass and charge, respectively); $f^0(u) \equiv f(u)$ is the isotropic part of the electron distribution function, identified with the EEDF in the framework of the two-term approximation, and satisfying the normalisation condition $\int_0^\infty f(u)\sqrt{u}du = 1$; and $f^1(u)$ is the (real part of the) first-anisotropy of the electron distribution function.

Under the previous conditions, the EBE including a non-conservative collisional operator can be written as

$$\sqrt{\frac{m_e}{2eu}}\frac{\langle\nu_{\rm eff}\rangle}{N}uf(u) + \frac{1}{N}\sqrt{\frac{m_e}{2e}}\frac{dG(u)}{du} = S(u) \tag{3a}$$

$$f^1(u) = -\frac{\zeta\,(E/N)}{\Omega_{\rm PT}(u)}\frac{df(u)}{du} \quad , \tag{3b}$$

or

$$\frac{1}{3}\frac{\alpha_{\rm eff}}{N}uf^1(u) + \frac{1}{N}\sqrt{\frac{m_e}{2e}}\frac{dG(u)}{du} = S(u) \tag{4a}$$

$$f^1(u) = -\frac{(\alpha_{\rm eff}/N)}{\Omega_{\rm SST}(u)}f(u) - \frac{(E/N)}{\Omega_{\rm SST}(u)}\frac{df(u)}{du} \quad , \tag{4b}$$

where $(3a)$ and $(4a)$ or $(3b)$ and $(4b)$ correspond to the isotropic and anisotropic components of the EBE, respectively, in the following approximations: the space-homogeneous equations $(3a)$-$(3b)$ assume an exponential temporal growth of the electron density with a growth constant $\langle\nu_{\rm eff}\rangle \equiv \langle\nu_{\rm ion}\rangle - \langle\nu_{\rm att}\rangle \equiv \sum_{k,i}\delta_{k_i}\left[\langle\nu_{k_i,{\rm ion}}\rangle - \langle\nu_{k_i,{\rm att}}\rangle\right]$, corresponding to the electron net creation frequency for the system under study (with $\langle\nu_{\rm ion}\rangle$ and $\langle\nu_{\rm att}\rangle$ the corresponding electron mean frequencies for ionisation and attachment, respectively, and where the sums extend over all levels of all gases in the mixture); the time-constant equations $(4a)$-$(4b)$ assume an exponential spatial growth of the electron density in the direction opposite to that of the applied electric field, with a growth constant $\alpha_{\rm eff} \equiv \alpha - \eta \equiv \sum_{k,i}\delta_{k_i}\left(\alpha_{k_i} - \eta_{k_i}\right)$, corresponding to the effective electron Townsend coefficient (with α and η the corresponding first and second Townsend coefficients for ionisation and attachment, respectively). Note that the inclusion of growth models for the electron density is necessary if one intends a space and time independent description, yet including non-conservative collisional mechanisms such as electron ionisation and attachment. The temporal growth model was used to simulate Pulsed Townsend (PT) discharges by Tagashira *et al* [65], using the formulation of Thomas [66] for the one dimensional continuity equation of electrons under the action of an uniform electric field. The spatial growth model is usually adopted when simulating Steady State Townsend (SST) discharges maintained with a DC electric field [65].

Equations $(3a)$-$(3b)$ can be used in either the DC or the HF cases, whereas equations $(4a)$-$(4b)$ are for the DC case only. In these equations, the quantity E/N is the *reduced electric field*, where $E \equiv E_p/\zeta$ (with $\zeta = 1$ or $\sqrt{2}$ for the DC or the HF cases, respectively); the quantities $\Omega_{\rm PT}$ and $\Omega_{\rm SST}$ have the dimensions of a cross section,

being defined as

$$\Omega_{\rm PT}(u) \equiv \Omega_c(u) + \frac{[m_e/(2eu)]\,(\omega/N)^2}{\Omega_c(u)} \tag{5a}$$

$$\Omega_{\rm SST}(u) \equiv \sigma_c(u) \quad , \tag{5b}$$

where $\Omega_c(u) \equiv \sigma_c(u) + \sqrt{m_e/(2eu)}\,(\langle\nu_{\rm eff}\rangle/N)$, with $\sigma_c(u) \equiv \sum_k \chi_k \sigma_{k,c}$ the electron-neutral total momentum-transfer cross section, for the system under study, and $\sigma_{k,c}$ the corresponding cross section for gas k; $G \equiv G_E + G_{\rm el} + G_{\rm CAR} + G_{ee}$ is the *upflux* function that contains power gain/loss contributions due to, in order, the applied electric-field, the elastic collisions, the rotational collisions (in the continuous approximation for rotations, CAR, with a Chapman-Cowling correction due to the gas temperature [57, 67–69], written here for the case of homonuclear diatomic molecules), and the electron-electron collisions [68], respectively

$$G_E(u) = N\sqrt{\frac{2e}{m_e}}\frac{u}{3}\frac{1}{\zeta}\frac{E}{N}f^1(u) \tag{6a}$$

$$G_{\rm el}(u) = -\sum_k 2\gamma_k \nu^{\rm el}_{k,c}(u)u^{3/2}\left[f(u) + \frac{k_B T_g}{e}\frac{df(u)}{du}\right] \tag{6b}$$

$$G_{\rm CAR}(u) = -\sum_k 4B_k \nu_{0,k} u^{1/2}\left[f(u) + \frac{k_B T_g}{e}\frac{df(u)}{du}\right] \tag{6c}$$

$$G_{ee}(u) = -2\nu_{ee}(u)u^{3/2}\left[I(u)f(u) + J(u)\frac{df(u)}{du}\right] \quad , \tag{6d}$$

where $\gamma_k \equiv m_e/M_k$, $\nu^{\rm el}_{k,c} \equiv N_k\sqrt{2eu/m_e}\,\sigma^{\rm el}_{k,c}$ is the electron-neutral elastic momentum-transfer collision frequency for the gas k ($\sigma^{\rm el}_{k,c}$ being the corresponding cross section), $\nu_{0,k} \equiv N_k\sqrt{2eu/m_e}\,\sigma_{0,k}$ is the electron-neutral collision frequency for the rotational excitation of gas k ($\sigma_{0,k} \equiv 8\pi Q_k^2 a_0^2/15$ being the corresponding cross section, with a_0 the Bohr radius), B_k and Q_k are the rotational constant and the quadrupole-moment constant (in units of ea_0^2) of the gas k, respectively, $I(u)$ and $J(u)$ are the relevant Spitzer integrals [39, 70], and $\nu_{ee} \equiv 4\pi\left[e^2/(4\pi\varepsilon_0 m_e)\right]^2 \ln\Lambda_c/v^3 n_e$ is the electron-electron collision frequency (with ε_0 the vacuum permittivity, $\ln\Lambda_c$ the Coulomb logarithm ($\Lambda_c \equiv 12\pi n_e \lambda_D^3$) and λ_D the Debye length); $S \equiv \sum_{i,j>i} S_{i,j} + \sum_i S_{i,\rm ion} + \sum_i S_{i,\rm att}$ is the discrete collision operator that contains power loss/gain contributions due to inelastic/superelastic mechanisms, ionisation and attachment, respectively

$$\begin{aligned} S_{i,j}(u) &= \delta_i\left[(u+V_{i,j})\sigma_{i,j}(u+V_{i,j})f(u+V_{i,j}) - u\sigma_{i,j}(u)f(u)\right] \\ &\quad + \delta_j\frac{g_i}{g_j}\left[u\sigma_{i,j}(u)f(u-V_{i,j}) - (u+V_{i,j})\sigma_{i,j}(u+V_{i,j})f(u)\right] \end{aligned} \tag{7a}$$

$$\begin{aligned} S_{i,\rm ion}(u) = \delta_i\Bigg\{&\int_{u+V_{i,\rm ion}}^{2u+V_{i,\rm ion}} u'\sigma^{\rm sec}_{i,\rm ion}(u', u'-V_{i,\rm ion}-u)f(u')du' \\ &+ \int_{2u+V_{i,\rm ion}}^{\infty} u'\sigma^{\rm sec}_{i,\rm ion}(u',u)f(u')du' - u\sigma_{i,\rm ion}(u)f(u)\Bigg\} \end{aligned} \tag{7b}$$

$$S_{i,\rm att}(u) = -\delta_i u\sigma_{i,\rm att}(u)f(u) \quad . \tag{7c}$$

In (7*a*)-(7*c*), the levels i, j and the reduced densities δ_i, δ_j now refer to any level for any gas in the system; $\sigma_{i,j}$ is the electron-collision cross section for the $i \to j$ excitation with energy threshold $V_{i,j}$ and statistical weights g_i and g_j, respectively (note that the third and fourth superelastic terms in (7*a*) were written resorting to the Klein-Rosseland relation [71]); $\sigma_{i,\mathrm{att}}(u)$ is the electron-collision cross section for the attachment of level i; $\sigma^{\mathrm{sec}}_{i,\mathrm{ion}}(u', u)$ is the single differential cross section (SDCS) for the ionisation of level i with energy threshold $V_{i,\mathrm{ion}}$; and

$$\sigma_{i,\mathrm{ion}}(u) = \int_0^{(u-V_{i,\mathrm{ion}})/2} \sigma^{\mathrm{sec}}_{i,\mathrm{ion}}(u, u')du' \tag{8}$$

is the integral cross section for the ionisation of level i. The SDCS takes into account the distribution of the energy available after an ionisation event, caused by a primary electron with energy u', yielding a secondary electron born in the event with energy u and a scattered electron with energy $u' - V_{i,\mathrm{ion}} - u$.

Note that the effect of rotational inelastic/superelastic mechanisms, in the electron kinetics of homonuclear diatomic molecules, can be considered by adopting either the CAR approach of (6*c*) or the discrete approach of the collision operator (7*a*), yielding similar results provided that the rotational constants Q_k and B_k are coherently matched to the rotational cross section set $\sigma_{i,j}$ [57].

LoKI-B allows the user to choose between different descriptions of the ionisation mechanism, namely: (i) taking ionisation as a conservative mechanism, described by the inelastic part of the collisional operator (7*a*), in which case the first terms in the left-hand side of (3*a*) and (4*a*) should be set to zero; (ii) taking ionisation as a non-conservative mechanism, described by the collisional operator (7*b*) with a SDCS, and using the EBE given by (3*a*)-(4*b*); (iii) taking ionisation as a non-conservative mechanism, and prescribing no-sharing of energy between the secondary electron, introduced at $u = 0$, and the scattered electron, introduced at energy $u' - V_{i,\mathrm{ion}}$. In this case the SDCS for the secondary electrons writes $\sigma^{\mathrm{sec}}_{i,\mathrm{ion}}(u', u) = \sigma_{i,\mathrm{ion}}(u')\delta(u)$ and the ionisation operator becomes

$$\begin{aligned} S_{i,\mathrm{ion}}(u) = \delta_i \Big[& (u + V_{i,\mathrm{ion}})\sigma_{i,\mathrm{ion}}(u + V_{i,\mathrm{ion}})f(u + V_{i,\mathrm{ion}}) - u\sigma_{i,\mathrm{ion}}(u)f(u) \\ & + \sqrt{\frac{m_e}{2e}}\frac{\langle \nu_{i,\mathrm{ion}} \rangle}{N}\delta(u)\Big] \quad , \end{aligned} \tag{9}$$

corresponding to the inelastic part of (7*a*) plus an extra term that describes the introduction of new electrons at zero-energy; (iv) taking ionisation as a non-conservative mechanism, and prescribing equal-energy-sharing between the secondary and the scattered electrons, introduced at energy $(u' - V_{i,\mathrm{ion}})/2$. In this case the SDCS for the secondary electrons writes $\sigma^{\mathrm{sec}}_{i,\mathrm{ion}}(u', u) = \sigma_{i,\mathrm{ion}}(u')\delta[u - (u' - V_{i,\mathrm{ion}})/2]$ and the ionisation operator becomes

$$\begin{aligned} S_{i,\mathrm{ion}}(u) = \delta_i \big[& 4(2u + V_{i,\mathrm{ion}})\sigma_{i,\mathrm{ion}}(2u + V_{i,\mathrm{ion}})f(2u + V_{i,\mathrm{ion}}) \\ & - u\sigma_{i,\mathrm{ion}}(u)f(u)\big] \quad , \end{aligned} \tag{10}$$

where the first term of $S_{i,\mathrm{ion}}(u)du$ describes the entrance of both the secondary and the scattered electrons at a total energy between $2u$ and $2u + 2du$, produced by a primary

electron with energy $u' = 2u + V_{i,\mathrm{ion}}$, whereas the second term describes the exit of primary electrons with energy u after ionizing collisions.

Note that the current version of LoKI-B does not include any external sources of electrons, such as electron beam injection or photoionization. However, the model adopted in the code can be easily upgraded as to consider these effects: (i) on the right-hand side of the EBE, with the addition, to the source function S, of an energy-resolved gain-term; (ii) on the left-hand side of the EBE, with the addition of the corresponding energy-integral term, describing the growth of the electron density in a stationary situation. The inclusion of these external sources of electrons, as well as the handling of the non-conservative electron-collision mechanisms (particularly the attachment), must be carefully monitored in all cases, since they can be responsible for the development of significant anisotropies, in which case the two-term expansion of the EBE adopted here is no longer valid.

3.2. Cross section models adopted

LoKI-B adopts specific models to define the total momentum-transfer cross section, σ_c, and the SDCS for the ionisation of level i, $\sigma_{i,\mathrm{ion}}$.

The momentum-transfer cross section, for an electron-neutral collision described by a differential (angle-resolved) cross section $\sigma(u,\theta)$, is generally defined as [72]

$$\sigma_c(u) \equiv 2\pi \int_0^\pi \sigma(u,\theta)(1-\cos\theta)\sin\theta d\theta \quad . \tag{11}$$

For a gas k, the electron-neutral momentum-transfer cross section $\sigma_{k,c}(u)$ is constructed by weighting the contributions of the different types of collisional mechanisms to give

$$\sigma_{k,c}(u) = \sum_i \xi_{k_i}\sigma^{\mathrm{el}}_{k_i,c}(u) + \sum_{i,j>i}\left[\xi_{k_i}\sigma_{k_{(i,j)},c}(u) + \xi_{k_j}\sigma_{k_{(j,i)},c}(u)\right] \quad , \tag{12}$$

where $\sigma^{\mathrm{el}}_{k_i,c}$, $\sigma_{k_{(i,j)},c}$ and $\sigma_{k_{(j,i)},c}$ are the electron-neutral momentum-transfer cross sections for the elastic scattering of level k_i, the inelastic excitation $k_i \to k_j$, and the superelastic de-excitation $k_j \to k_i$, respectively. The latter cross sections, whose magnitudes are usually much smaller than those of $\sigma^{\mathrm{el}}_{k_i,c}$, are often taken assuming an isotropic scattering (also due to the lack of data), in which case one can identify the momentum-transfer cross section with the integral cross section (integrated over all scattering angles), i.e. $\sigma_{k_{(i,j)},c} \simeq \sigma_{k_{(i,j)}}$. Also, the elastic momentum-transfer cross section is usually identified with that of the highly-populated ground-state of the gas. Therefore

$$\sigma_{k,c}(u) \simeq \sigma^{\mathrm{el}}_{k,c}(u) + \sum_{i,j>i}\left[\xi_{k_i}\sigma_{k_{(i,j)}}(u) + \xi_{k_j}\sigma_{k_{(j,i)}}(u)\right] \quad . \tag{13}$$

The solution of the EBE (3*a*)-(4*b*) requires information on both the elastic and the total momentum-transfer cross sections, but the way to obtain it depends on the momentum-transfer data available for each gas. If the elastic momentum-transfer cross section is available, equation (13) can be used directly to deduce the corresponding total $\sigma_{k,c}$, knowing the electron-scattering inelastic / superelastic cross sections for the

transitions considered together with the relevant populations, to be self-consistently determined (if possible) within a kinetic model. Conversely, if the data available is for a total momentum-transfer cross section, which in databases is usually termed as *effective* $\sigma^{\rm eff}_{k,c}$ (see section 3.3), then the elastic momentum-transfer cross section can be deduced from $\sigma^{\rm el}_{k,c} = \sigma^{\rm eff}_{k,c} - \sum_{i,j>i}\left[\xi^{\rm prescribed}_{k_i}\sigma_{k_{(i,j)}} + \xi^{\rm prescribed}_{k_j}\sigma_{k_{(j,i)}}\right]$, where the populations $\xi^{\rm prescribed}_{k_i}$ and $\xi^{\rm prescribed}_{k_j}$ correspond to some prescribed distribution, coherent with the measured / estimated data of $\sigma^{\rm eff}_{k,c}$, and allowing to obtain a *unique* result (density independent) for the elastic cross section. By default, LoKI-B adopts a Boltzmann distribution at the gas temperature for $\xi^{\rm prescribed}_{k_i}$, but the user can modify this choice. The previous comments support the recommendation of replacing, whenever possible, the data for effective momentum-transfer cross sections with that for elastic momentum-transfer cross sections.

The implementation of the ionisation operator (7*b*) requires information on the SDCS, discriminating its values as a function of the primary and the secondary electron energies. In general, the available experimental data for SDCS is scarce and often measured for only a few energy values of the primary electron. Here, we have adopted the comprehensive set of measurements of Opal *et al* [73], for the double differential cross section of different gases, resolved on both the energy and the angle of the secondary electron. This pioneering work proposes differential ionization cross sections with a very reliable shape [74], which can be normalized from available experimental data for the corresponding integral cross sections (see (8)). Indeed, after integration over the angles, and by comparing the energy distributions of the secondary electrons for different energies of the primary electrons, these authors proposed a fitting expression for the SDCS

$$\sigma^{\rm sec}_{i,{\rm ion}}(u',u) = \frac{\sigma_{i,{\rm ion}}(u')}{w\arctan\left[\left(u'-V_{i,{\rm ion}}\right)/(2w)\right]}\frac{1}{1+(u/w)^{\beta}} \quad , \tag{14}$$

where $\beta \simeq 2$ and w is a parameter close to the ionisation threshold $V_{i,{\rm ion}}$, which is set for each gas according to the original estimates [73]. Note that (14) satisfies exactly the expression (8) for the integral cross section $\sigma_{i,{\rm ion}}$, and therefore it is used in LoKI-B to describe the energy distribution of the electrons involved in ionisation events, using available data (see section 3.3) and mitigating possible normalisation errors. Note also that (14) is not the sole fitting expression proposed for the SDCS in the literature, a possible alternative being given in [75].

3.3. Input data

LoKI-B solves the EBE (3*a*)-(4*b*) given: the working conditions E/N (or T_e, when choosing a generalised Maxwellian as EEDF, see section 3.5), p, T_g, $\omega/2\pi$ and n_e, along with: the χ_k fractions of the various k-gases in the mixture; the distributions of populations ξ_{k_i}, $\xi_{k_{i_v}}$ and $\xi_{k_{i_{v_J}}}$ of electronic levels k_i, vibrational levels k_{i_v} and rotational levels $k_{i_{v_J}}$, respectively (if applicable); and the sets of cross sections $\sigma^{\rm el}_{k_i,c}$ (or $\sigma^{\rm eff}_{k,c}$, see section 3.2), $\sigma_{i,j}$ and $\sigma_{i,{\rm ion}}$, where here i,j stand for any level of any gas in the

system. Note that T_g is needed to calculate the elastic and the CAR operators (6b) and (6c), whereas p is required to calculate the total gas density in the particular case of HF excitations (for obtaining the reduced frequency ω/N) and/or if electron-electron collisions are considered in the calculations (for obtaining the ionisation degree n_e/N).

Input parameters are set from a text input-file, in a user-friendly flexible way, e.g. allowing to (i) prepare simulations for either a sole value or a range of values of the applied reduced electric field or electron temperature; (ii) choose among different ionisation models (conservative, no-sharing or equal-energy-sharing) and electron-density growth models (temporal or spatial); (iii) define the distributions of populations directly in the input file, from user-defined text files, or via functions for typical distributions at user-defined temperatures (e.g. Boltzmann or Treanor); (iv) list the filename(s) with the set(s) of cross sections to adopt in the simulations; (v) provide details about the energy grid and the solution algorithm to adopt in the simulations (see section 3.4). The code uses SI units for all physical quantities, except the energies that are expressed in eV (electron-volt) and the reduced fields that are expressed in Td (Townsend; 1 Td = 10^{-21} Vm^2).

By default, LoKI-B uses electron scattering cross sections obtained from the LXCat open-access website [38]. The cross sections can be assembled into a single file, or given from multiple files. As input, LoKI-B accepts also *extra* sets of cross sections, which are *not* used in the calculation of the EEDF, but remain available for integration over the calculated EEDF, to obtain electron macroscopic parameters with interest for various purposes (e.g. global models, spectroscopy analysis, actinometry diagnostics, etc.). The choice of the input data is the responsibility of the users, meaning that the selection of any cross section set (obtained or not from LXCat) must be carefully validated and evaluated according to the specific needs and the conditions of interest for the simulations.

LXCat is organised to provide "data required for modeling low temperature plasmas" [38] in the most effective way. In the case of electron-neutral scattering cross sections, LXCat provides easy access to *complete sets* of cross sections, defined as those giving a good description of all electron energy and momentum losses [72], yielding electron swarm parameters in agreement with available measured data (within experimental uncertainties), when used in a two-term Boltzmann solver [72, 76]. Each *complete set* assembles cross sections for electron collisions with different neutral targets, usually associated with the electronic ground-state of each gas. To date, on LXCat these data are tagged with the name of the corresponding gas (e.g. `Ar`, `N2`, `O2`, `CO2`, $\cdots$) and are grouped under the category `Ground states`, where one can find cross sections for the collisions of electrons with the electronic / vibrational / rotational ground-states of a neutral gas. For example, the datasets `N2` may contain (i) the elastic / effective momentum-transfer cross section for N_2; (ii) excitation cross sections for different electronic levels (including the ionisation level), from the electronic ground-state N_2(X); (iii) excitation cross sections for different vibrational levels N_2(X,v), from the vibrational ground-state N_2(X,v= 0); (iv) a global rotational excitation cross section

for N_2(X).

This practical organisation of LXCat can create some difficulties when a detailed discrimination and handling of data is intended. The reason is of technical nature, and it relates with the fact that, to date, electron collisions with the `Ground state` of a gas are described as a collection of mechanisms `e + gas name -> ···`, with no possibility to specify the internal structure of the electronic ground-state of the gas. To circumvent this limitation, LoKI-B checks the free-field `COMMENT`, of the LXCat datasets, to look for details on the full structure of reactants and products, for each electron-impact reaction. This workaround is the practical solution to prepare any cross section datafile obtained from LXCat for use in LoKI-B, and it is already implemented in the database IST-Lisbon. For example, in IST-Lisbon the v=0 to v=1 vibrational excitation within ground-state N_2(X) is described by LXCat metadata as `e + N2 -> e + N2(v=0 - v=1)`, but is discriminated in the `COMMENT` field as `e + N2(X,v=0) -> e + N2(X,v=1)`. Note also that, in IST-Lisbon, the cross sections for excitations from vibrational levels N_2(X,v> 0) and from rotational levels N_2(X,v=0,J), can be found in the datasets termed `N2-vib` and `N2-rot`, respectively.

3.4. Numerical solution

The EBE is numerically solved in an uniform energy grid $u_n = (n - 1/2)\Delta u$, defined in the energy interval $[0, u_{\max}]$ with $n = 1, 2, \cdots \mathcal{N}$ cells of fixed step-size $\Delta u = u_{\max}/\mathcal{N}$, each cell n being limited by nodes $n - 1/2$ and $n + 1/2$. The user can define the energy grid in two ways: (i) by setting the maximum energy $u_{\max}$ and the number of cells $\mathcal{N}$; (ii) by prescribing a number of decades in the fall of the EEDF, between f_1 and $f_{\mathcal{N}}$, as to ensure an automatic adjustment of the energy grid. Typical values for the decade-fall are within 10 to 25, considering not only the use of double precision, but also the order of magnitude of the various quantities (kinetic energy, cross sections) multiplying the EEDF in the calculations. The user is responsible for adequately defining the energy grid, namely by noticing that small energy steps are required to resolve any relevant structure in the cross sections, such as near-threshold variations and resonances, as well as situations involving the presence of a Ramsauer minimum.

Equations $(3a)$-$(4b)$ are written for each grid-cell, where the isotropic and anisotropic functions f and f^1 are defined, with the corresponding upfluxes G_x ($x = E, \mathrm{el}, \mathrm{CAR}, ee$) and cross sections σ_y ($y = k, c\,; k_{(i,j)}$) being set on the grid-nodes. The cross sections are interpolated linearly from the data provided by the user, setting to zero all the values up to the corresponding energy threshold, i.e. $\sigma_{y_n} = 0$ for $n \leq$ `INT` $(V_{i,j}/\Delta u)$.

The EBE is discretised adopting the finite differences scheme presented in [9]. The result is a system of algebraic equations that can be written under matrix form, with tridiagonal elements coming from the left-hand sides of $(3a)$ and $(4a)$, and some sparse off-tridiagonal elements due to the electron-neutral collisional operator in the right-hand sides. In particular, equations $(3a)$-$(4b)$ are composed by terms proportional to f, df/du

and dG/du whose discretised forms can be generally summarised as follows

$$
\begin{aligned}
&[a(u)f(u)]_n &&= a_n f_n && (15a)\\
&[a'(u)f(u \pm V_{i,j})]_n &&= a'_n f_{n \pm \mathrm{INT}(V_i,j/\Delta u)} && (15b)\\
&\left[b(u)\frac{df(u)}{du}\right]_n &&= b_n \frac{f_{n+1} - f_{n-1}}{2\Delta u} && (15c)\\
&\left.\frac{dG_x(u)}{du}\right|_{n;\, x=E,\mathrm{el,CAR}} &&= \left\{\frac{d}{du}\left[g_x(u)\left(f(u) + c\frac{df(u)}{du}\right)\right]\right\}_n \\
& &&= \left[\frac{g_{x_{n-1/2}}}{\Delta u}\left(\frac{c}{\Delta u} - \frac{1}{2}\right)\right] f_{n-1} \\
& &&- \left[\frac{g_{x_{n+1/2}}}{\Delta u}\left(\frac{c}{\Delta u} - \frac{1}{2}\right) + \frac{g_{x_{n-1/2}}}{\Delta u}\left(\frac{c}{\Delta u} + \frac{1}{2}\right)\right] f_n \\
& &&+ \left[\frac{g_{x_{n+1/2}}}{\Delta u}\left(\frac{c}{\Delta u} + \frac{1}{2}\right)\right] f_{n+1} && (15d)\\
&\left.\frac{dG_{ee}(u)}{du}\right|_n &&= \left\{\frac{d}{du}\left[\mathcal{I}(u)f(u) + \mathcal{J}(u)\frac{df(u)}{du}\right]\right\}_n \\
& &&= A_{n-1}f_{n-1} - (A_n + B_n)\, f_n + B_{n+1}f_{n+1} \quad , && (15e)
\end{aligned}
$$

where $a(u)$, $a'(u)$ and $b(u)$ are generic functions of u; c is a constant; $g_x(u)$, $\mathcal{I}(u)$ and $\mathcal{J}(u)$ can be obtained straightforwardly from (6a)-(6d); and the coefficients A_n and B_n are linear functions of the EEDF given by

$$
A_n = -\frac{\mathcal{I}_{n+1/2}}{2\Delta u} + \frac{\mathcal{J}_{n+1/2}}{(\Delta u)^2} \equiv \sum_{m=1}^{\mathcal{N}} a_{n,m} f_m \qquad (16a)
$$

$$
B_n = \frac{\mathcal{I}_{n-1/2}}{2\Delta u} + \frac{\mathcal{J}_{n-1/2}}{(\Delta u)^2} \equiv \sum_{m=1}^{\mathcal{N}} b_{n,m} f_m \quad . \qquad (16b)
$$

The previous equations are subjected to the following conditions [9]: (i) the flux boundary conditions $G(0) = G(u_{\max}) = 0$, which imply $g_{x_{1/2}} = g_{x_{\mathcal{N}+1/2}} = 0$ and $A_0 = A_{\mathcal{N}} = B_1 = B_{\mathcal{N}+1} = 0$; (ii) the energy conservation condition for dG_{ee}/du, which yields $a_{n,m} = b_{m,n}$; and (iii) the imposition of a Maxwellian EEDF for $dG_{ee}/du = 0$, which is ensured by setting $a_{n,m} = a_{m-1,n+1}$.

After discretisation, the isotropic part of the EBE can be written as $\sum_{m=1}^{\mathcal{N}} C_{n,m}(f) f_m = 0$, which is solved coupled to the normalisation condition $\sum_{m=1}^{\mathcal{N}} f_m \sqrt{u_m}\Delta u = 1$. The matrix $C(f)$ is nonlinear due to the presence of the following terms. First, the temporal/spatial growth-term of the electron density, associated with non-conservative mechanisms, involves either the effective ionisation rate coefficient $\langle \nu_{\mathrm{eff}} \rangle / N$ or the effective Townsend reduced coefficient α_{eff}/N, both being functions of the EEDF (see section 3.5). Second, the expression of the electron-electron upflux G_{ee} involves linear functions of the EEDF, as confirmed by (6d) and (16a)-(16b).

In the absence of nonlinear effects (e.g., for electropositive gases, with the ionization taken as a conservative mechanism and no electron-electron collisions), the EBE is solved adopting a very effective direct solution method. Conversely, when the matrix $C(f)$

contains nonlinear terms, the EBE must be solved using some iterative method. In the case of weak nonlinear effects (e.g., low electronegativity and low ionization degree), the solution can be obtained by using two nested iterative algorithms, based on successive direct solutions. The algorithms adopt (i) a mixing of solutions to converge over $\langle\nu_{\rm eff}\rangle/N$ or $\alpha_{\rm eff}/N$, looking for relative differences of these parameters below $10^{-9}-10^{-10}$, between two consecutive iterations; (ii) a Newton-Raphson-based approach to converge over the ratio of the power "dissipated" in electron-electron collisions to the power gained from the applied electric field Θ_{ee}/Θ_E, looking for values of this ratio below $10^{-9}-10^{-10}$. Final convergence demands also relative variations of the EEDF below 10^{-11}, between two consecutive iterations. In the case of strong nonlinear effects, the user is recommended to choose a relaxation method for solving the EBE. Here, the default convergence criterion demands relative variations of the EEDF below 10^{-10}, between two consecutive iterations.

3.5. The electron macroscopic parameters

On output, LoKI-B calculates the isotropic and the anisotropic parts of the electron distribution function, in addition to various electron macroscopic parameters obtained by integration over the EEDF, namely: (i) swarm parameters (transport parameters and rate coefficients), which can be used to adjust complete sets of electron-scattering cross sections [47, 76] or as input parameters in macroscopic (fluid / global) plasma models [1, 77, 78]; (ii) power-transfer terms [1, 70], providing the distribution of power among the different collisional channels and controlling the calculation errors.

The rate coefficients for excitation / de-excitation mechanisms, between levels i and $j > i$, are given by [1]

$$C_{i,j} = \sqrt{\frac{2e}{m_e}} \int_0^\infty u\sigma_{i,j}(u) f(u) du \tag{17a}$$

$$C_{j,i} = \sqrt{\frac{2e}{m_e}} \int_0^\infty \frac{g_i}{g_j}(u + V_{i,j})\sigma_{i,j}(u + V_{i,j}) f(u) du \quad . \tag{17b}$$

Note that (17a)-(17b) can be applied not only to the cross sections adopted for solving the EBE, but also to the *extra* set of cross sections defined by the user as additional input data of LoKI-B (see section 3.3).

The ionisation and the attachment rate coefficients are defined similarly to (17a) as

$$C_{i,\rm ion} \equiv \frac{\langle\nu_{i,\rm ion}\rangle}{N} = \sqrt{\frac{2e}{m_e}} \int_0^\infty u\sigma_{i,\rm ion}(u) f(u) du \tag{18a}$$

$$C_{i,\rm att} \equiv \frac{\langle\nu_{i,\rm att}\rangle}{N} = \sqrt{\frac{2e}{m_e}} \int_0^\infty u\sigma_{i,\rm att}(u) f(u) du \quad . \tag{18b}$$

For simulations involving the time-growth of the electron density, equations (18a)-(18b) are solved within each iteration on the convergence parameter $\langle\nu_{\rm eff}\rangle/N$ (see section 3.4).

The reduced transverse free-diffusion coefficient and the reduced mobility are calculated from [1, 70]

$$D_e N = \frac{1}{3}\sqrt{\frac{2e}{m_e}}\int_0^\infty \frac{u}{\Omega_x(u)} f(u)du \tag{19a}$$

$$\mu_e N = -\frac{1}{3}\sqrt{\frac{2e}{m_e}}\int_0^\infty \frac{u}{\Omega_x(u)}\frac{df(u)}{du}du \quad . \tag{19b}$$

In (19a), $x = c, \mathrm{SST}$ for temporal or spatial growth of the electron density, respectively. Equation (19b) corresponds either to the DC mobility, at $\omega = 0$ and $x = \mathrm{PT}, \mathrm{SST}$ for temporal or spatial growth of the electron density, respectively; or to the real part of the HF mobility, at $\omega \gg \nu_c$ and $x = \mathrm{PT}$. Equations (3b) and (4b) can be integrated to define the electron mean drift velocity $v_d \equiv \sqrt{2e/m_e}\int_0^\infty (u/3) f^1(u)du$, yielding

$$v_d = \mu_e E \ , \ \text{for a PT situation} \tag{20a}$$

$$v_d = \mu_e E - D_e \frac{1}{n_e}\frac{dn_e}{dz} = \mu_e E - D_e \alpha_{\mathrm{eff}} \ , \ \text{for a SST situation} \quad , \tag{20b}$$

and equation (4a) can be integrated to define the effective Townsend coefficient

$$\alpha_{\mathrm{eff}} = \frac{\langle \nu_{\mathrm{ion}} \rangle - \langle \nu_{\mathrm{att}} \rangle}{v_d} = \frac{\langle \nu_{\mathrm{eff}} \rangle}{v_d} \quad . \tag{21}$$

For DC simulations involving the spatial-growth of the electron density, equations (20b) and (21) can be combined to yield

$$D_e \alpha_{\mathrm{eff}}^2 - \mu_e E \alpha_{\mathrm{eff}} + \langle \nu_{\mathrm{eff}} \rangle = 0 \quad , \tag{22}$$

and in this case (22) is solved within each iteration on the convergence parameter α_{eff} (see section 3.4).

The balance equation for the electron power-density, per electron at unit gas density, is obtained by multiplying (3a) or (4a) by $u\sqrt{2e/m_e}$ and integrating it over all energies. The result writes (in eV s^{-1} m^3)

$$\frac{\Theta_{\mathrm{growth}}}{N} + \frac{\Theta_E}{N} + \frac{\Theta_{\mathrm{coll}}^{\mathrm{gain}}}{N} + \frac{\Theta_{\mathrm{coll}}^{\mathrm{loss}}}{N} = 0 \quad , \tag{23}$$

where the different terms represent, in order, the variation of the power density due to non-conservative mechanisms inducing a time/space net growth of the electron density, the power density gained from the applied electric field, and the power density gained/lost in collisional events, respectively

$$\frac{\Theta_{\mathrm{growth}}}{N} = \begin{cases} -\frac{\langle \nu_{\mathrm{eff}} \rangle}{N}\varepsilon \ , \ \text{for a PT situation} \\ -\frac{\alpha_{\mathrm{eff}}}{N}\left(\mu_\varepsilon E - D_\varepsilon \alpha_{\mathrm{eff}}\right) \ , \ \text{for a SST situation} \end{cases} \tag{24a}$$

$$\frac{\Theta_E}{N} = \frac{v_d}{\zeta}\frac{E}{N} \tag{24b}$$

$$\frac{\Theta_{x=\mathrm{el,CAR}}^{\mathrm{gain}}}{N} = -\int_0^\infty g_x(u) c \frac{df(u)}{du}du \tag{24c}$$

$$\frac{\Theta_{ee}^{\mathrm{gain}}}{N} = -\int_0^\infty \mathcal{J}(u)\frac{df(u)}{du}du \tag{24d}$$

$$\frac{\Theta^{\text{gain}}_{\text{sup}}}{N} = \sum_{i,j>i} \delta_j C_{j,i} V_{i,j} \tag{24e}$$

$$\frac{\Theta^{\text{loss}}_{x=\text{el,CAR}}}{N} = -\int_0^\infty g_x(u) f(u) du \tag{24f}$$

$$\frac{\Theta^{\text{loss}}_{ee}}{N} = -\int_0^\infty \mathcal{I}(u) f(u) du \tag{24g}$$

$$\frac{\Theta^{\text{loss}}_{\text{inel}}}{N} = -\sum_{i,j>i} \delta_i C_{i,j} V_{i,j} \quad . \tag{24h}$$

In these equations, the labels "inel" and "sup" refer to inelastic and superelastic collisions, respectively, associated with rotational, vibrational, electronic excitation / de-excitation and ionisation mechanisms. In (24a), $\varepsilon \equiv \int_0^\infty u^{3/2} f(u) du$ is the electron mean energy, and D_ε and μ_ε are the diffusion coefficient and the mobility for the electron-energy flux, respectively, defined by expressions similar to (19a) and (19b) where the integrand function is further multiplied by u.

The parameters defined by (17a)-(24h) can be calculated adopting the distribution function $f(u)$, as obtained from the solution to the EBE, or some prescribed EEDF, such as a generalised Maxwellian [79–81]

$$f(u) = \left(\frac{2}{3k_B T_e}\right)^{3/2} \frac{\Gamma(\frac{5}{2s})^{3/2}}{\Gamma(\frac{3}{2s})^{5/2}} \exp\left[-\left(\frac{\Gamma(\frac{5}{2s})}{\Gamma(\frac{3}{2s})} \frac{2eu}{3k_B T_e}\right)^s\right] \quad , \tag{25}$$

where Γ represents the gamma-function, T_e is the electron kinetic temperature such that $(k_B T_e)/e \equiv (2/3)\varepsilon$, and s is a positive real number that allows shaping the EEDF. In particular, (25) yields a Maxwellian EEDF and a Druyvesteyn EEDF for $s = 1$ and $s = 2$, respectively.

3.6. Validity limits and control

The two-term approximation adopted in LoKI-B to solve the EBE is valid in a situation of small anisotropies [1], corresponding to electron–neutral mean-free-paths much smaller than any characteristic dimension of the plasma container, and an energy gain from the electric field, between collisions, much smaller than the electron kinetic energy. For a homogeneous scenario like the one described here, the latter condition is the most relevant and can be approximately written as (see (20a) and (24b))

$$\Theta_E \sim \mu_e E^2 \ll \varepsilon \nu_c \quad , \tag{26}$$

which yields, for a Maxwellian EEDF at 1 eV temperature and a typical reduced collision frequency $\nu_c/N \sim \sigma_c \langle v \rangle \sim 10^{-19} \times 10^6 = 10^{-13}$ m^3 s^{-1}, $E/N \ll \sqrt{m_e \varepsilon / e}(\nu_c/N) \sim$ 300 Td. This is a conservative limit for the reduced electric-field, often exceeded in calculations because the two-term approximation yields fairly good results still. However, users are advised to check the EEDF results when taking E/N values much above the estimated validity limit, namely by comparing the solution obtained for the isotropic and the anisotropic parts of the electron distribution function. Also, HF

calculations are valid only if the oscillation frequency of the electric field is much larger than the typical frequency for the electron energy relaxation, which can be approximately written as (see (6*b*))

$$\omega \gg \gamma N(\nu_c/N) \quad , \tag{27}$$

corresponding to $\omega/(2\pi) \gg 20$ MHz - 20 kHz for $\nu_c/N \sim 10^{-13}$ m^3 s^{-1}, $\gamma \sim 5 \times 10^{-5}$, $T_g = 300$ K and $p \sim 10^5$ Pa - 130 Pa. Again, users are advised to check the validity of the HF approximation for the particular working conditions considered.

LoKI-B contains several control features upon the input data and the calculation results, and in some cases it returns warning messages for the benefit of users. In particular: (i) the code controls the maximum value $u_{\max}$ of the energy grid adopted, comparing it with the cutoff energy u_{cutoff} of the electron-neutral elastic momentum-transfer cross section. When $u_{\text{cutoff}} < u_{\max}$ a warning message is returned, and if the user accepts to proceed with the calculations these are carried out by setting to zero the values of any cross section from its corresponding u_{cutoff} and up to $u_{\max}$. LoKI-B does not extrapolate cross sections beyond the cutoff energies defined in the input data-files, again because it adopts an ontology that separates the tool and the data. The user is recommended to always careful examine the cross sections being used and, if needed, he/she should adopt adequate laws to extrapolate them, chosen according to the specific processes considered (e.g. dipole allowed or dipole forbidden electron excitation, ionization, etc); (ii) the code returns a warning message if the calculation of the elastic momentum-transfer cross section from the corresponding effective produces negative values for $\sigma^{\text{el}}_{k,c}$ (see section 3.2), which is then set to zero. In this case, users are advised to check the cross section data adopted; (iii) the code controls the quality of the Boltzmann-matrix inversion, by monitoring the error upon the fractional electron power-balance. The latter is obtained from (23), by normalizing this equation with respect to a *reference power-density* Θ_{ref}, defined for each calculation as the sum of all power-gain terms (24*b*), (24*c*), (24*e*). The relative error $\left[\Theta_E + \Theta^{\text{gain}}_{\text{coll}} + \Theta^{\text{loss}}_{\text{coll}} + \Theta_{\text{growth}}\right]/\Theta_{\text{ref}}$ (with typical value $\sim 10^{-10}$) degrades for very-low E/Ns, due to the smallness of the power-density values for all the power-transfer channels, and for very-high E/Ns, if the $u_{\max}$ grid-limit adopted in the calculations is not large enough to prevent ill-conditioned EBE-matrices.

4. Results

This section gives examples of results obtained with LoKI-B for different gases. The examples were chosen to serve a twofold purpose. First, they illustrate the roadmap followed in the development of the simulation tool, which involves its verification against analytical results, its benchmarking against numerical calculations obtained with other codes, and the validation of the results obtained by comparison with available measurements of swarm parameters. Second, they put forward the main features and the flexibility of operation of LoKI-B. The verification and the benchmarking exercises

are carried out for model gases, whereas the validation procedure uses real data from atomic and molecular gases, or for gas mixtures. Calculations are for given values of E/N at $\omega = 0$, considering a gas temperature of 300 K, using the SDCS given by (14) to describe the energy sharing between the scattered and the secondary electrons after each ionisation, and assuming a temporal growth of the electron density, unless stated otherwise. Typical run times are found between $0.5 - 1$ s, depending of the E/N value considered, for calculations done in a laptop with a single processor at ~ 3.5 GHz, adopting an energy grid with $\mathcal{N} = 1000$ cells adjusted as described in section 3.4.

4.1. Examples for model gases

An obvious verification of LoKI-B corresponds to the solution of the EBE for a model gas where the sole electron-scattering mechanisms are elastic collisions with the neutrals. The problem can be solved analytically, yielding the well-known Margenau EEDF [82]

$$f(u) \propto \exp\left[-\int_0^u \frac{du'}{\frac{e}{3\gamma m_e}\left(\frac{E/N}{\nu_c^{\rm el}/N}\right)^2 + \frac{k_B T_g}{e}}\right] \quad , \tag{28}$$

and for a constant momentum-transfer rate coefficient the result is a Maxwellian EEDF at temperature

$$T_{e,\rm Mxw} \equiv T_g + \frac{1}{3k_B\gamma m_e}\left(\frac{eE/N}{\nu_c^{\rm el}/N}\right)^2 \quad . \tag{29}$$

For this verification test we consider a model gas with $\nu_c^{\rm el}/N = 10^{-12}$ m^3 s^{-1} and $M = 40$ amu, running LoKI-B for E/N values between 0 and 50 Td, adjusting the maximum value of the energy grid as to ensure a fall of 15 decades for the EEDF (see section 3.4). Figure 1 shows the EEDF and the ratio of the anisotropic-to-isotropic components of the electron distribution function, at $E/N = 10$ Td (corresponding to $k_B T_e/e = 4.53$ eV) and $\mathcal{N} = 1000$ cells. As expected, the anisotropic component of the electron distribution function increases with the electron energy, yet remaining below the isotropic part.

To evaluate quantitatively the deviation of the EEDF with respect to a Maxwellian distribution function, $f_{\rm Mxw}$, one can follow different approaches. The simplest is to monitor the differences of the electron kinetic temperatures obtained from the curve in fig. 1 and calculated from (29), $\Delta T_e/T_{e,\rm Mxw} \equiv |T_e - T_{e,\rm Mxw}|/T_{e,\rm Mxw}$. One can also compare directly the numerical and the analytical EEDFs, as shown in fig. 2, which presents the relative error between the distribution functions and the mean value of this error over the entire kinetic-energy scale, $\overline{\Delta f/f_{\rm Mxw}} \equiv \overline{|f_{\rm numerical}(u) - f_{\rm Mxw}(u)|/f_{\rm Mxw}(u)}$. Note that the steady increase in the relative error of $f(u)$, as the kinetic energy increases, is due to the division by an exponentially decreasing function, as was confirmed by calculating the corresponding absolute errors. The relative errors for T_e and $f(u)$ are plotted in fig. 3, as a function of E/N at constant $\mathcal{N} = 1000$ cells, revealing small standard deviations σ around average values $\langle . \rangle$ between 5×10^{-4} and 10^{-3} respectively: $\langle \Delta T_e/T_{e,\rm Mxw} \rangle \pm \sigma_{T_e} = 5.33 \times 10^{-4} \pm 10^{-6}$ and $\langle \overline{\Delta f/f_{\rm Mxw}} \rangle \pm \sigma_f = 1.57 \times 10^{-3} \pm 8 \times 10^{-6}$.

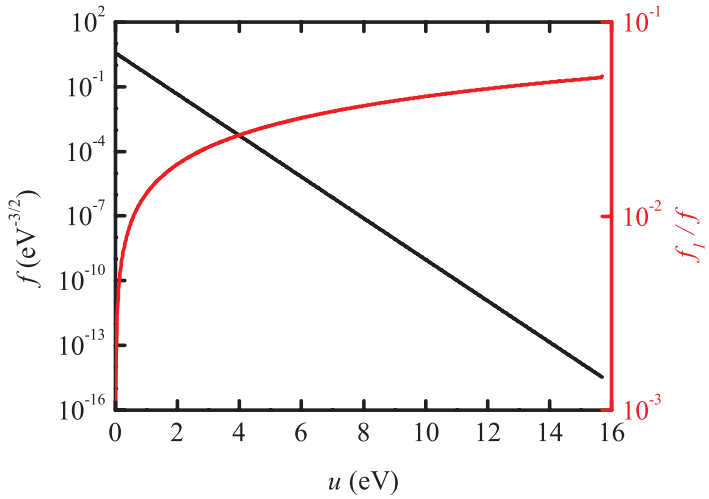

Figure 1. Electron energy distribution function (black curve, left axis) at E/N = 10 Td and $\mathcal{N}$ = 1000 cells, calculated with LoKI-B for a model gas where the sole electron-scattering mechanisms are elastic collisions with the neutrals, assuming a constant momentum-transfer rate coefficient [82]. For comparison purposes, the figure shows also the ratio of the anisotropic-to-isotropic components of the electron distribution function (red, right).

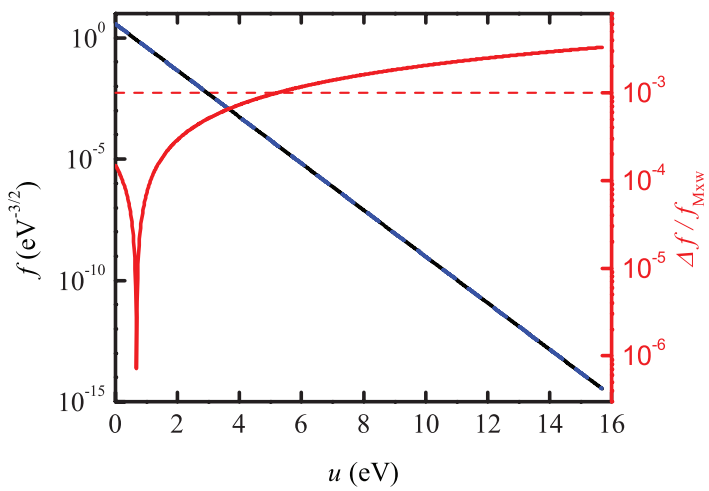

Figure 2. Analytical (solid black curve) and numerical (dashed blue) EEDFs (see left axis), calculated for the same conditions as in fig. 1. The figure shows also the relative error between the distribution functions (solid red curve), and the mean value of the error over the entire kinetic-energy scale (dashed red) (see right axis).

The small error-dispersion observed in fig. 3 is preserved for other values of $\mathcal{N}$ but, as expected, it is possible to decrease the relative error by increasing the number of grid-cells. Figure 4 shows the evolution of the average relative error for the electron temperature and the EEDF, as a function of the number of grid-cells, and from the data in this log-log representation one can estimate the order of the algorithm adopted in the calculations. Indeed, the slope of the trend line with the squares is approximately 2, which is coherent with the use of a second-order-accurate discretization scheme in

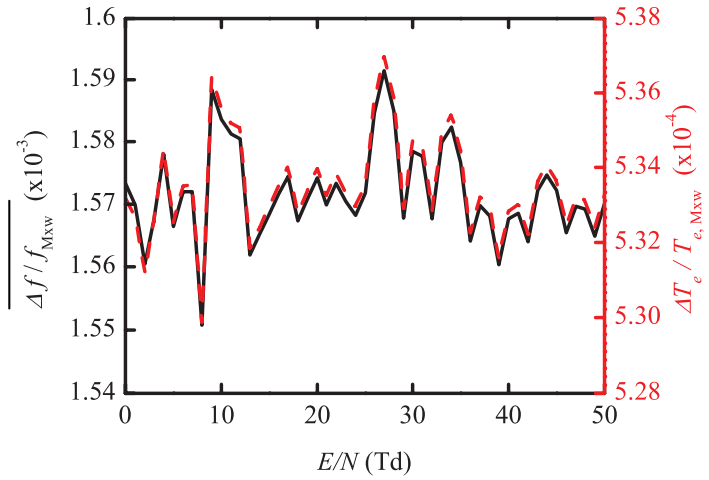

Figure 3. Relative error of the EEDF (solid black curve, left axis) and the electron temperature (dashed red, right), as a function of the reduced electric field, calculated at $\mathcal{N} = 1000$ cells for the same conditions as in fig. 1.

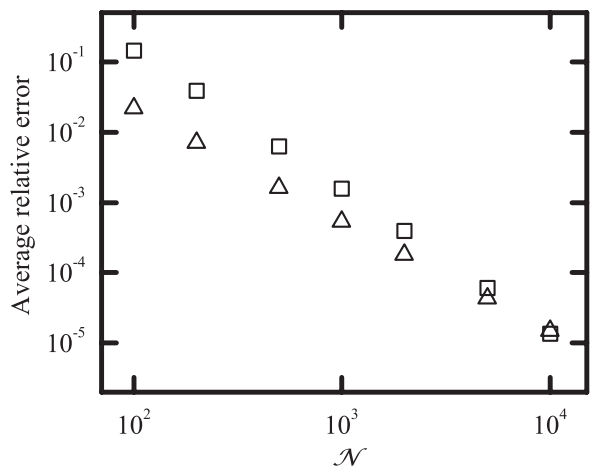

Figure 4. Average relative error of the electron temperature (triangles) and the EEDF (squares), as a function of the number of grid-cells, evaluated for different E/N values under the same conditions as in fig. 1.

,

solving the EBE, whereas the slope of the trend line with the triangles is roughly 1.6, thus revealing that the evaluation of the electron temperature is related not only with the discretization scheme adopted for the EBE, but also with the integration routine used to obtain macroscopic values from the EEDF (first-order mid-point quadrature rule).

A second verification check of LoKI-B analyses the behavior of the electron-electron collision operator (6*d*) for an increasing influence of these collisions, namely due to an increase in the electron density. For this verification check we consider a Reid-type model gas [43] with mass $M = 4$ amu, temperature $T_g = 300$ K and the following electron-scattering cross sections: *constant* elastic momentum-transfer cross

section $\sigma_c^{\rm el} = 6 \times 10^{-20}$ m^2; *ramp* inelastic cross section with threshold 0.2 eV and slope 10^{-19} m^2 eV^{-1}. Figure 5 shows the EEDF calculated at $E/N = 10$ Td and $\mathcal{N} = 1000$ cells, for electron densities varying between 10^{17} and 10^{22} m^{-3}, corresponding to ionisation degrees $n_e/N = 10^{-6}$–10^{-1} at $p = 414$ Pa and $T_g = 300$ K. As expected, the

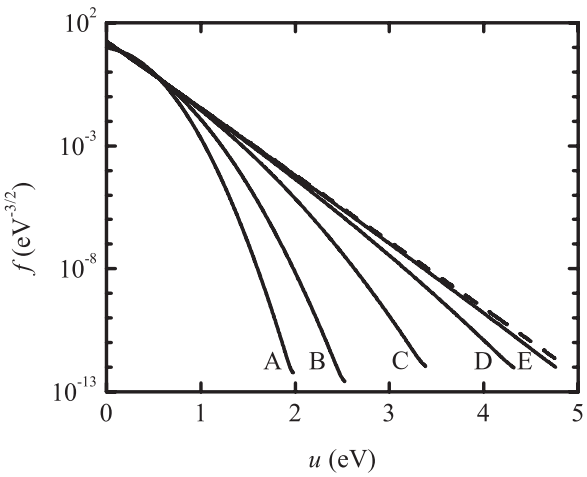

Figure 5. Electron energy distribution function, calculated with LoKI-B for a Reid ramp-model [43] at $E/N = 10$ Td, $T_g = 300$ K, $p = 414$ Pa and $\mathcal{N} = 1000$ cells, including the effects of electron-electron collisions for the following ionisation degrees: 10^{-5} (A), 10^{-4} (B), 10^{-3} (C), 10^{-2} (D), 10^{-1} (E). The dashed curve is a Maxwellian distribution function at $k_B T_e/e = 0.16$ eV, corresponding to the electron kinetic temperature of the EEDF calculated for $n_e/N = 0.1$.

EEDF approaches a Maxwellian distribution function with the increase in the ionisation degree, which confirms the correct behavior for the operator G_{ee}.

The development of LoKI-B involves also its benchmarking against numerical calculations obtained with other codes, namely the very popular BOLSIG+ [27]. For these comparisons we have adopted the same Reid model gas as before [43], except for the value of the gas temperature taken equal to 0 K, according to the definition settings of this model gas. The calculations consider E/N values between 1 and 100 Td, adopting an energy grid with $\mathcal{N} = 1000$ cells, adjusted as to ensure a 13 decade-fall for the EEDF. Figure 6(a)-(b) shows, as a function of E/N, the electron reduced mobility, as the example of an electron macroscopic parameter calculated with LoKI-B and BOLSIG+, and the relative difference between the predictions of the codes for $\mu_e N$, $D_e N$ and ε. In general, the results obtained with LoKI-B and BOLSIG+ are in good agreement, within errors of $10^{-2}\% - 1\%$ ($\langle \Delta X/\langle X\rangle\rangle \pm \sigma_X = 2.20 \times 10^{-3} \pm 3 \times 10^{-6}, 4 \times 10^{-4} \pm 3 \times 10^{-4}, 2 \times 10^{-3} \pm 2 \times 10^{-3}$, for $X = \mu_e N, D_e N, \varepsilon$, respectively).

4.2. Example for an atomic gas: argon

As mentioned previously (see section 3.5), swarm parameters can be used to adjust complete sets of electron-scattering cross sections, and this procedure of code/data

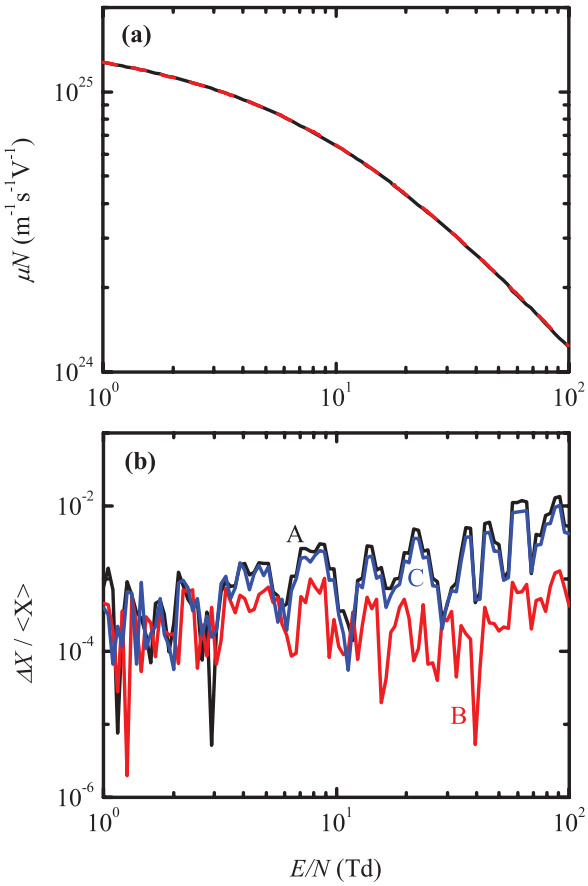

Figure 6. Example of benchmark of LoKI-B against BOLSIG+, for a Reid ramp-model [43]. (a) Electron reduced mobility, as a function of the reduced electric field, calculated using LoKI-B (solid black curve) and BOLSIG+ (dashed red). (b) Relative difference between the predictions of the two codes, as a function of the reduced electric field, for the electron reduced mobility (black A curve), the electron free-diffusion coefficient (red B) and the electron mean energy (blue C).

validation was also adopted in the development of LoKI-B, by comparing calculation results with available measurements for these parameters.

As an example for an atomic gas, fig. 7(a)-(b) shows, as a function of E/N, calculations and measurements of the electron reduced mobility and the electron characteristic energy $u_k \equiv D_e/\mu_e$ of argon, obtained for $T_g \simeq 300$ K, 77 K. LoKI-B calculations used the `Ar` complete set of cross sections, published in the IST-Lisbon database of LXCat [83]. The results in this figure reproduce the typical validation agreement between calculations and measurements, within the experimental uncertainty.

Argon was used also to analyse the impact, on the EEDF and the electron swarm parameters, of the different descriptions available for the ionisation (see section 3.1): using a *SDCS* given by (14), according to Opal's model [73]; prescribing specific distributions of the energy available after each ionisation, between the secondary and the scattered electrons, namely by assuming *no-sharing* of energy with the secondary electron or *equal-energy-sharing* between both electrons; taking ionisation

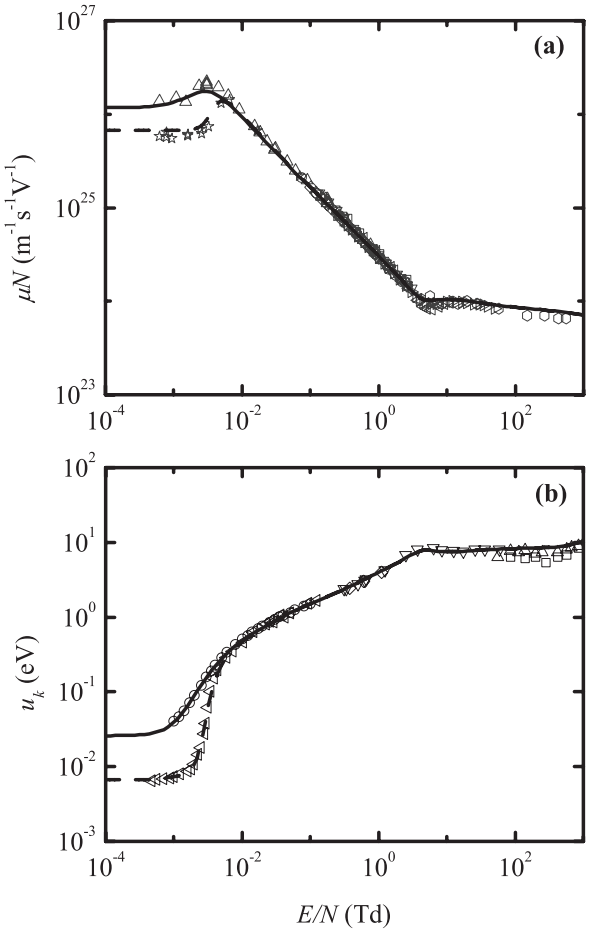

Figure 7. Electron swarm parameters in argon, as a function of the reduced electric field. The lines are calculations with LoKI-B for $T_g = 300$ K (solid curves) and 77 K (dashed). The points are experimental data, retrieved from the IST-Lisbon, Dutton and LAPLACE datatases with LXCat [83–85]. (a) Reduced mobility. The points are from the following authors: Nielsen [86] (□); Bowe [87] (○); Pack and Phelps [88] (△); Wagner *et al* [89] (▽); Robertson [90] (◇); Christophorou *et al* [91] (◁); Nakamura and Kurachi [92] (▷); Kucukarpaci *et al* [93] (⬡); Pack and Phelps [88] (77 K, ☆); (b) Characteristic energy. The points are from the following authors: Lakshminarshima *et al* [94] (□); Milloy *et al* [95] (294 K, ○); Al-Amin *et al* [96] (△); Townsend and Bailey [97] (288 K, ▽); Warren and Parker [98] (77 K, ◇).

as a *conservative* mechanism, with no production of secondary electron. Figure 8(a)-(b) plots the EEDF at $E/N = 300$ Td and the first reduced Townsend coefficient as a function of E/N, for an argon plasma. LoKI-B calculations used the IST-Lisbon cross section set, and adopted the four descriptions mentioned above for the ionisation mechanism, assuming a spatial-growth of the electron density when considering the production of secondary electrons due to ionisation events.

An observation of fig. 8(a) shows the following: (i) for all non-conservative descriptions, regardless of the specific energy-sharing-model adopted (SDCS, no-sharing or equal-energy-sharing), the introduction of secondary electrons at low energies is responsible for an enhancement of the body of the EEDF and a simultaneous depletion

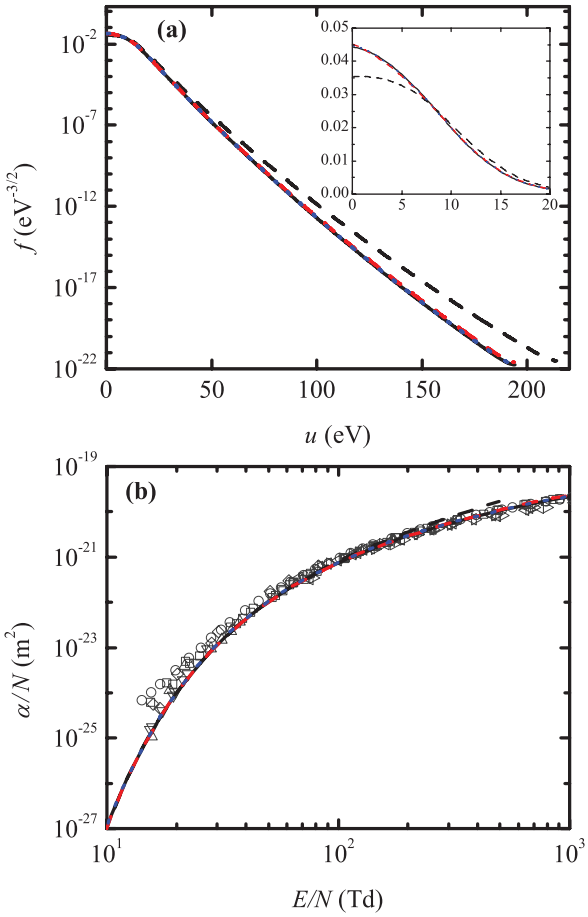

Figure 8. Electron energy distribution function, calculated with LoKI-B for argon plasmas at $E/N = 300$ Td, adopting the following descriptions for the energy sharing in electron-impact ionisations: conservative (dashed-black curve); non-conservative, equal-energy-sharing (solid-black); non-conservative, using a SDCS (dotted-blue); non-conservative, no-sharing (dashed-red). The non-conservative descriptions assume a spatial-growth of the electron density. The insert is a zoom of the EEDF over the low-energy region. (b) First reduced Townsend coefficient, as a function of the reduced electric field, for argon plasmas. The lines are calculations with LoKI-B for the same conditions as in (a). The points are experimental data, retrieved from the IST-Lisbon datatase with LXCat [83], from the following authors: Kruithof and Penning [99] (□); Kruithof [100] (○); Golden and Fisher [101] (△); Specht [102] (▽); Abdulah (from Puech and Torchin [103]) (◇); Jelenak *et al* [104] (◁); Bozin *et al* [105] (▷).

of its tail, as to yield a normalised distribution; (ii) the description no-sharing, given by (9), produces the highest enhancement of the EEDF, in the region close to $u = 0$. This description is partly identical to the treatment of electron-impact ionisations as a conservative mechanism, the difference being associated with the introduction of secondary electrons at zero energy. In this case the scattered electrons have the largest possible energy $u' - V_{\rm ion}$, causing the EEDF tail to be slightly above all other solutions for non-conservative descriptions; (iii) both SDCS and equal-energy-sharing descriptions induce a larger distribution of energy between the secondary and the scattered electrons,

leading to the corresponding decrease of the EEDF in the region close to $u = 0$.

The changes observed in the EEDF have consequences upon the swarm parameters, namely the first Townsend coefficient. Figure 8(b) shows that, as expected for high E/N, the calculated values of α/N are smaller (and in better agreement with the available measurements), when electron-impact ionisations are described as a non-conservative mechanism.

4.3. Example for a molecular gas: nitrogen

The procedure of validation of a complete set of electron-scattering cross sections using swarm parameters was applied also to molecular gases. For example, fig. 9 shows, as a function of E/N, calculations and measurements of the electron reduced mobility of nitrogen, obtained for $T_g \simeq 300$ K. LoKI-B calculations used the `N2` complete set of

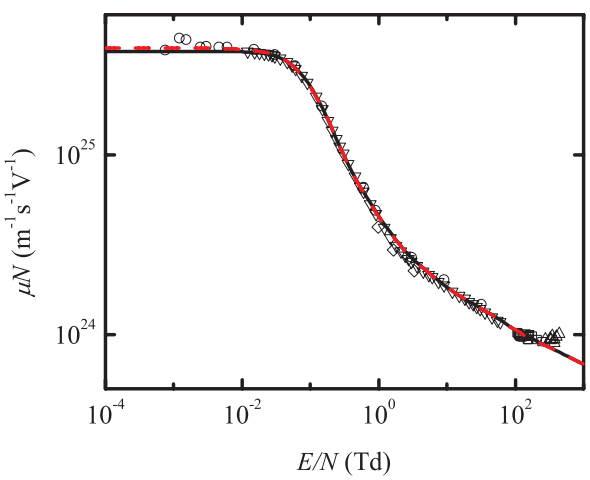

Figure 9. Electron reduced mobility in nitrogen, as a function of the reduced electric field. The lines are calculations with LoKI-B for $T_g \simeq 300$ K, where rotational excitations / de-excitations are described adopting either the continuous approximation for rotations (CAR, solid black curve) or a discrete approach (dashed red) that considers transitions involving the levels N_2(X,v=0,J=0-32). The points are experimental data, retrieved from the IST-Lisbon datatase with LXCat [106], from the following authors: Frommhold [107] (□); Pack and Phelps [88] (○); Wagner and Raether [108] (△); Lowke [109] (293 K, ▽); Errett (from Engelhardt *et al* [110]) (293 K, ◇).

electron-scattering cross sections, published in the IST-Lisbon database of LXCat [106]. The `N2` cross sections describe the elastic momentum-transfer due to electron collisions with the ground-state N_2(X); the excitation of electronic levels $N_2(A^3\Sigma_u^+$, $B^3\Pi_g$, $W^3\Delta_u$, $B^3\Sigma_u^-$, $a^1\Sigma_u^-$, $a^1\Pi_g$, $w^1\Delta_u$, $C^3\Pi_u$, $E^3\Sigma_g^+$, $a^1\Sigma_g^+$, higher-singlets) from the ground-state N_2(X); the excitation of vibrational levels N_2(X,v=1-10) from the vibrational ground-state N_2(X,v=0); and the ionisation of N_2(X). For simulations at low E/N values, the dataset `N2` is complemented with the description of the rotational excitation / de-excitation of the ground-state N_2(X,v=0) by electron impact, i.e. e + N_2(X,v=0,J) $\leftrightarrow$ e + N_2(X,v=0,J'). As mentioned, this description can adopt either the continuous (CAR)

approach, using the $G_{\rm CAR}$ rotational operator ($6c$), or a discrete approach that considers a set of cross sections for rotational transitions involving the levels N_2(X,v=0,J=0-32), which corresponds to the `N2-rot` dataset published also in the IST-Lisbon database. The results in fig. 9 reveal a good agreement between calculations and measurements, within the experimental uncertainty, also validating the equivalence between the continuous and the discrete descriptions of rotational excitation / de-excitation mechanisms for nitrogen.

Nitrogen plasmas can be used also to demonstrate the distribution of the electron energy between various gain/loss channels. Figure 10(a)-(b) plots, as a function of E/N, the fractional power-transfer $\Theta_x/\Theta_{\rm ref}$ due to the different phenomena considered in the EBE ($x = E, {\rm el}, {\rm inel}, {\rm sup}, {\rm growth}$), and the largest power-densities per electron at unit gas density Θ_x/N ($x = E, {\rm sup-rotational}$), respectively. LoKI-B calculations used the same data and rotational descriptions as before. Figure 10(a) discriminates between electron power-gain mechanisms (positive values) and electron power-loss mechanisms (negative) (see ($24a$)-($24h$)), and in the case of inelastic/superelastic electron collisions it further discriminates the various collisional channels, i.e., rotational, vibrational, electronic excitation / de-excitation, and ionisation. As indicated, the results in this figure are normalised to the sum of the different power-gain terms, $\Theta_{\rm ref}$ (see section 3.5 and 3.6). Here, $\Theta_{\rm ref} \simeq \Theta_{\rm sup-rotational}$ for $E/N < 0.1$ Td (when adopting the CAR approach) or $E/N < 1$ Td (when using the discrete approach for rotations), and above these field values $\Theta_{\rm ref} \simeq \Theta_E$, as can be confirmed from fig. 10(b) or by checking, for each E/N, which mechanism gives $\Theta_x/\Theta_{\rm ref} = 1$ in fig. 10(a). An observation of fig. 10(b) reveals that CAR yields a slightly smaller power-transfer to the rotational channel, which results in the relative differences depicted in fig. 10(a) between CAR and the discrete approach for rotations, in the range 0.1 Td $\lesssim E/N \lesssim$ 10 Td. As expected, for reduced electric fields above 1 Td the electron power-losses are dominated by the vibrational and the electronic collisional channels.

4.4. Example for mixtures of nitrogen-oxygen-argon

One of the main features of LoKI-B is the flexibility of operation with mixtures of atomic/molecular gases. This section presents results of the electron kinetics for nitrogen-oxygen and air-argon mixtures, including an example of validation of swarm parameters, the analysis of the effect of vibrational distribution functions (VDF) upon the EEDF, and the influence, on the EEDF and the electron power-transfer, of admixing dry-air to argon plasmas.

Figure 11 shows, as a function of E/N, calculations and measurements of the electron reduced mobility for dry-air (80% N_2 - 20% O_2), obtained for $T_g \simeq 300$ K. LoKI-B calculations used data published in the IST-Lisbon database of LXCat [106, 119], namely the `N2` and the `O2` complete sets of electron-scattering cross sections, complemented by the datasets `N2-rot` and `O2-rot` for the (discrete) description of rotational transitions. The information on the electron cross sections contained in

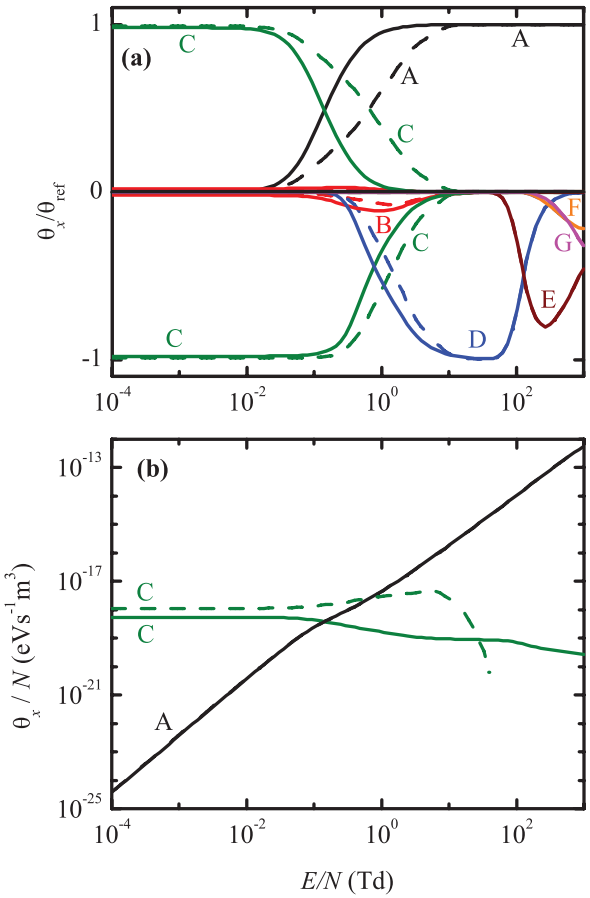

Figure 10. Electron power-transferred to various gain/loss channels in nitrogen, as a function of the reduced electric field, calculated with LoKI-B using either the continuous approximation for rotations (CAR, solid curves) or a discrete approach (dashed) that considers rotational transitions involving the levels N_2(X,v=0,J=0-32). (a) Fractional power-transfer due to the following phenomena: Joule heating (black curve A), elastic collisions (red B), rotational excitation / de-excitation (green C), vibrational excitation / de-excitation (blue D), electronic excitation / de-excitation (wine E), ionisation (orange F) and spatial growth (magenta G). The positive/negative values correspond to power gain/loss mechanisms. (b) Largest power-densities, per electron at unit gas density, obtained in the simulations of (a). The solid/dashed black A/green C curves correspond to the same gain mechanisms as in (a).

`N2` and `N2-rot` was already given in section 4.3. The `O2` cross sections include the elastic momentum-transfer due to electron collisions with the ground-state O_2(X); the excitation, from the ground-state O_2(X), of electronic levels $O_2(a^1\Delta_g, b^1\Sigma_g^+)$, $O_2(A^3\Sigma_u^+, C^3\Delta_u, c^1\Sigma_u^-)$ bound-states and leading to dissociation ($e + O_2(X) \rightarrow e + O(^3P) + O(^3P)$) and continuum Herzberg bands, $O_2(B^3\Sigma_u^-)$ leading to dissociation ($e + O_2(X) \rightarrow e + O(^3P) + O(^1D)$) and continuum Schumann-Runge bands, and O_2(9.97 eV,14.7 eV); the excitation of vibrational levels O_2(X,v=1-4) from the vibrational ground-state O_2(X,v=0); the electron dissociative attachment of O_2(X); and the ionisation of O_2(X). The `O2-rot` cross sections describe the rotational transitions by electron impact involving the levels O_2(X,v=0,J=1,3,5,$\cdots$,31), i.e. $e + O_2(X,v=0,J) \leftrightarrow e +$

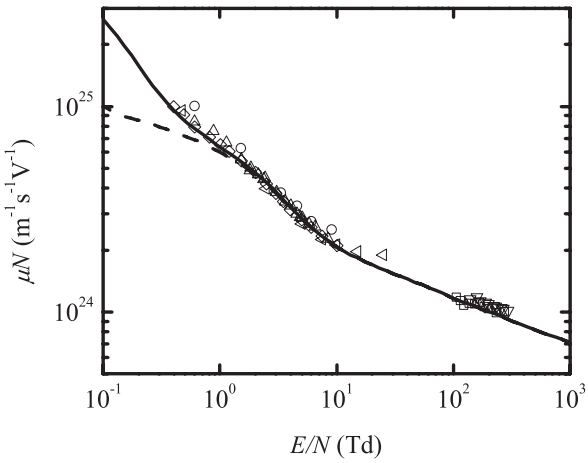

Figure 11. Electron reduced mobility in dry air (80% N_2 - 20% O_2), as a function of the reduced electric field. The lines are from calculations with LoKI-B for $T_g \simeq 300$ K, including (solid) or not including (dashed) rotational excitations / de-excitations involving the levels N_2(X,v=0,J=0-32) and O_2(X,v=0,J=1,3,5,$\cdots$,31). The points are experimental data, retrieved from the LAPLACE and Dutton datatases with LXCat [111, 112], from the following authors: Frommhold [113] (□); Hessenauer [114] (○); Nielsen *et al* [115] (△); Ryzko [116] (▽); Rees [117] (◇); Roznerski *et al* [118] (◁).

O_2(X,v=0,J+2). The results in fig. 11 reveal good agreement between calculations and measurements, within the experimental uncertainty. For comparison, fig. 11 shows also the results of μN in the absence of rotational transitions. Note that the inclusion of these mechanisms is essential to obtain a good agreement with the experiment, at low E/N. In particular, not considering these effects for N_2 (O_2) leads to an underestimation in the computed values of μN by 39% (8%), at 0.1 Td.

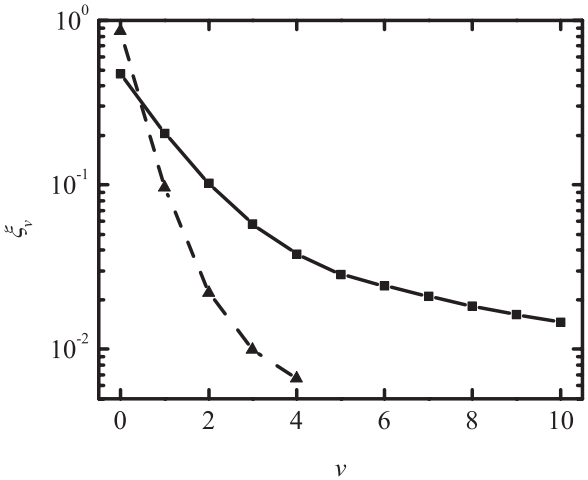

Figure 12. Vibrational distribution functions adopted in the calculations for nitrogen (solid curve and squares), corresponding to a Treanor-Gordiets distribution [120, 121] at $T_g = 300$ K and $T_{\rm vib} = 4000$ K, and for oxygen (dashed and triangles), corresponding to results recently calculated / measured in an oxygen ICP [122].

To analyse the effect of the vibrational transitions upon the EEDF, we have considered the VDFs plotted in fig. 12, corresponding to (i) a Treanor-Gordiets distribution [120, 121] at $T_g = 300$ K and $T_{\rm vib} = 4000$ K in nitrogen

$$\xi_v = \begin{cases} \exp\left\{-v\left[\frac{E_1-E_0}{k_B T_{\rm vib}} - (v-1)\frac{\Delta E}{k_B T_g}\right]\right\} & v \le v^\star \\ \xi_{v^\star}\frac{v^\star}{v} & v \ge v^\star \end{cases}, \tag{30}$$

with $v^\star = 1/2\,[1 + (E_1 - E_0)/\Delta E + T_g/T_{\rm vib}]$, where E_v $(v = 0, 1)$ is the energy of vibrational levels 0,1, and ΔE is the anharmonicity factor in eV; (ii) results recently calculated / measured in an oxygen ICP [122], which are representative of such distributions in O_2 regardless of the specific discharge conditions [123–125] .

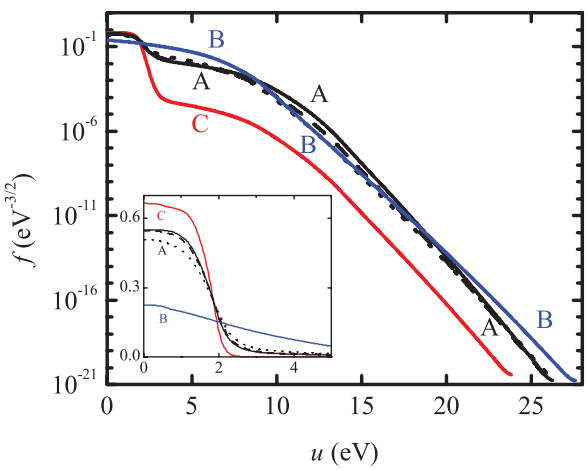

Figure 13. Electron energy distribution functions, calculated with LoKI-B at $E/N = 30$ Td, considering different N_2-O_2 mixtures with the VDFs plotted in fig. 12: 100% N_2 (A curve, black solid); 80% N_2 - 20% O_2 (A, black dashed); 50% N_2 - 50% O_2 (A, black dotted); 100% O_2 (B, blue). The C red curve is the EEDF calculated for 80% N_2 - 20% O_2, by setting to zero the population of all vibrational levels other than the ground-states N_2(X,v=0) and O_2(X,v=0). The insert is a zoom of the EEDF over the low-energy region.

Figure 13 shows EEDFs calculated with LoKI-B at $E/N = 30$ Td, considering different N_2-O_2 mixtures with the VDFs plotted in fig. 12. The results confirm the relevance of electron-vibrational excitation / de-excitation mechanisms in nitrogen, signalled by the sharp decrease in the body of the EEDF due to a vibrational barrier around 2 eV, which smooths down for increasing percentages of oxygen in the mixture (see the insert in this figure). Simulation results (not shown) confirm also that in oxygen, and for the working conditions considered, electron-vibrational mechanisms have little influence on the EEDF. As expected, the effect of vibrational *excitations* can be enhanced by setting to zero the populations of the excited vibrational levels, thus removing their influence as energy reservoirs for electron-impact superelastic collisions. The effect can be observed in fig. 13, by comparing the EEDFs obtained for air plasmas, either considering the VDFs of fig. 12 or by setting to zero the population of all vibrational levels other than the ground-states N_2(X,v=0) and O_2(X,v=0).

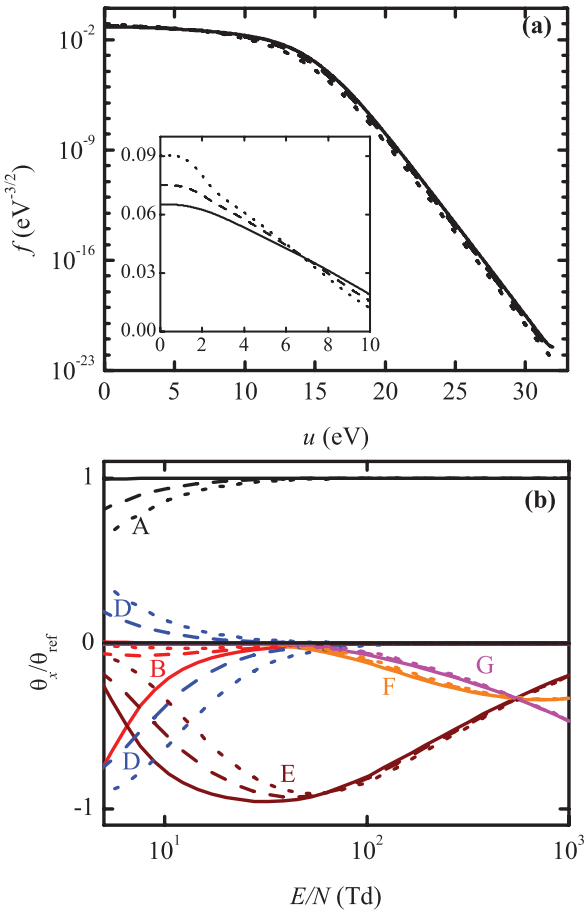

Figure 14. Electron energy distribution functions (at E/N = 30 Td) (a) and fractional power-transfer (b) calculated with LoKI-B, considering different mixtures of argon with dry-air (80% N_2 - 20% O_2): 100% Ar (solid curve); 98% Ar - 2% dry-air (dashed); 95% Ar - 5% dry-air (dotted). The calculations consider the VDFs plotted in fig. 12 for N_2 and O_2. The insert in (a) is a zoom of the EEDF over the low-energy region. The colors and labels in (b) correspond to the same power-transfer mechanisms as in fig. 10.

Figure 14(a)-(b) analyses the influence, on the EEDF (calculated at 30 Td) and the electron power-transfer, of admixing to argon plasmas a small percentage (below 5%) of dry-air (80% N_2 - 20% O_2, considering the VDFs plotted in fig. 12). As expected, the addition of air increases the relevance of the power transferred to vibrational transitions (with the corresponding decrease in the relative power transferred to elastic collisions and to electronic excitations, see fig. 14(b)), introducing a more distinctive separation between the EEDF regions below and above $\sim$ 2 eV (see fig. 14(a)), as consequence of the electron-impact vibrational excitations and de-excitations, respectively.

4.5. Example for an electric-field pulse applied to dry-air

The response of the electrons in a gas-mixture subjected to an electric-field pulse is a current hot topic in LTPs, mainly due to applications related with environmental

remediation, synthesis of value-added chemicals and new fuels, surface treatment and medicine [126–129].

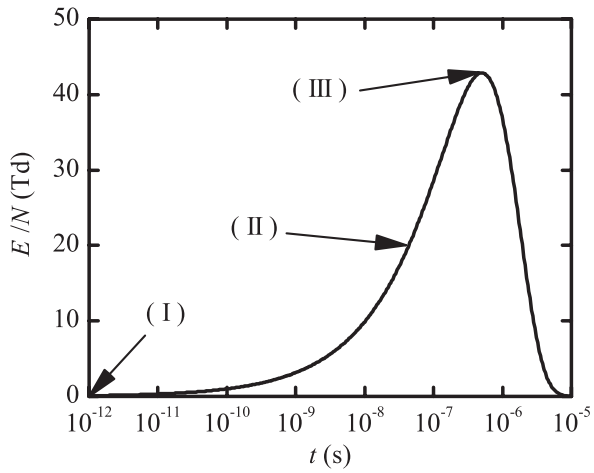

Figure 15. Plot of the electric-field temporal pulse given by (31).

In this context, LoKI-B was used to study the evolution in time of the electron kinetics, when an electric-field pulse with a duration of 10 μs is applied to a 80% N_2 - 20% O_2 gas mixture (dry-air). The simulations assume a time-dependent reduced electric-field (see fig. 15) given by

$$\frac{E(t)}{N} = \frac{E_0}{N}\sqrt{\frac{t}{t_0}}e^{-t/t_0} \quad , \tag{31}$$

with $E_0/N = 100$ Td and $t_0 = 1$ μs, taking as initial condition for the EEDF the zero-field solution of the EBE (which corresponds to a Maxwellian distribution at the gas temperature $T_g = 300$ K). Moreover, because LoKI-B handles the populations of excited states in a user-friendly way, the study considers the evolution of the EEDF in the presence of Boltzmann distribution functions, at $T_g = 300$ K, for the vibrational states N_2(X,v) and O_2(X,v) and for the rotational states N_2(X,v=0,J) and O_2(X,v=0,J), which are assumed not to change within the 10 μs time-interval of the simulations. The calculations were done following the same strategy adopted in several models [126–129], which consists in solving the time-independent EBE for a range of E/N to produce, as a function of either the reduced electric-field or the electron mean-energy, a table of rate coefficients that can be interpolated at different times during the execution of the model. Here, this *quasi-static approximation* was implemented by resolving the pulse rise into 500 E/N values, corresponding to time-steps below $\Delta t = 0.1$ μs.

For these working conditions, fig. 16(a)-(c) shows the evolution in time of the EEDF, calculated with LoKI-B at $E/N = 0, 20, 43$ Td, respectively, corresponding to the values signalled with arrows (I), (II) and (III) in fig. 15. Note that fig. 16(a) represents the initial condition for the EEDF; note also that the EEDFs in fig. 16(b)-(c) exhibit the vibrational barrier usually found in nitrogen plasmas, whose influence in the losses of the electron energy is mitigated with the increase in the electric-field intensity.

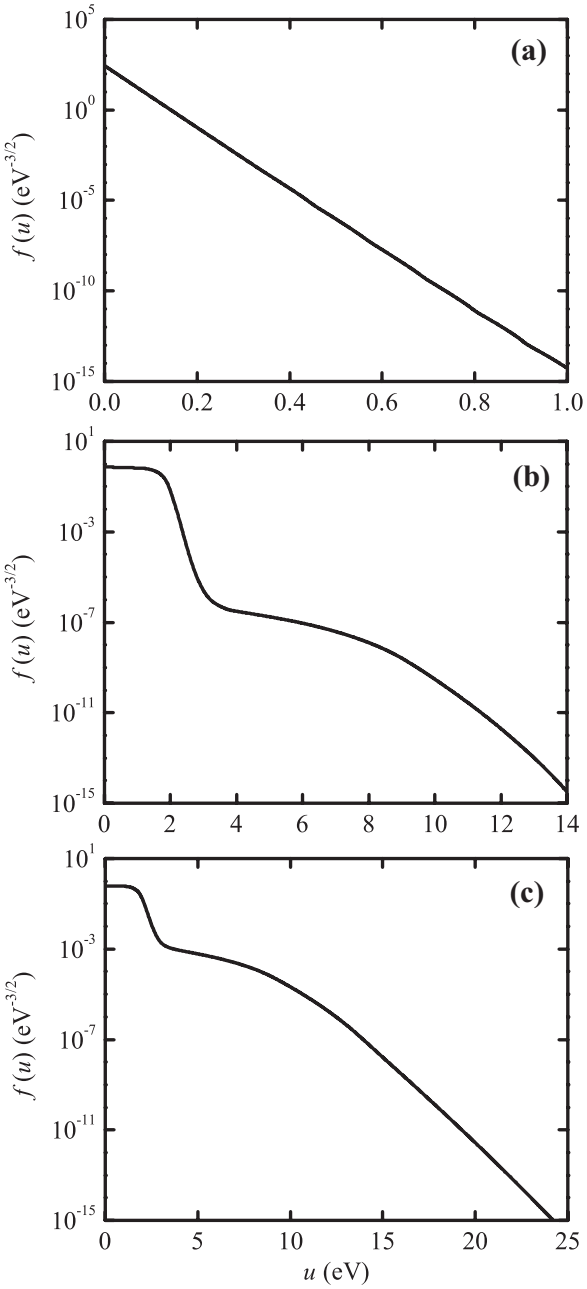

Figure 16. Electron energy distribution functions, calculated with LoKI-B at $E/N = 0$ Td (a), 20 Td (b) and 43 Td (c) (corresponding to the values signalled with arrows (I), (II) and (III) in fig. 15), for a 80% N_2 – 20% O_2 gas mixture (dry-air) at $T_g = 300$ K, considering Boltzmann distributions at 300 K for the vibrational and the rotational levels with the ground-states of nitrogen and oxygen.

The EEDFs calculated at different times can be used to obtain the time variation of pertinent electron macroscopic parameters, such as rate coefficients and power densities. For the same conditions as before, fig. 17(a)-(b) represents, as a function of time, the ionisation and the attachment rate coefficients, and the fractional power transferred from the electric field to the different electron-collision channels. Note the electronegative

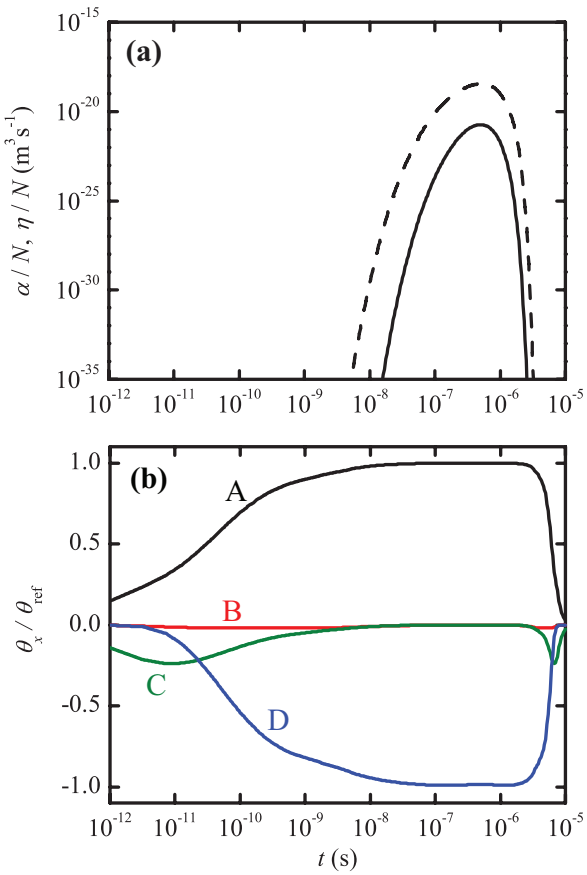

Figure 17. Electron rate coefficients (a) and most relevant fractional powers (b), calculated with LoKI-B as a function of time, for the electric-field temporal pulse of fig. 15 applied to a 80% N_2 - 20% O_2 gas mixture (dry-air) at T_g = 300 K, considering Boltzmann distributions at 300 K for the vibrational and the rotational levels with the ground-states of nitrogen and oxygen. The curves in this figure are for: (a), the ionisation (solid) and the attachment (dashed) rate coefficients; (b), Joule heating (black curve A), elastic collisions (red B), net rotational excitation (green C), net vibrational excitation (blue D). The positive/negative values correspond to power gain/loss mechanisms.

feature of the gas mixture, for which $\eta/N > \alpha/N$ during the whole duration of the pulse; note also that, as expected, the major power-transfer channels are due to rotational mechanisms (at low E/N) and vibrational mechanisms (at high E/N, namely around the electric-field peak).

The results presented here intend to demonstrate the flexibility of LoKI-B to exploit some relevant physical aspects related with the electron kinetics in LTPs. However, for what concerns the evolution in time of the EEDF, e.g. in reactive gas mixtures under the action of an electric-field pulse, a more cautious approached should be considered, involving the solution of the time-dependent EBE (instead of using a quasi-static approximation, based on the solution of its time-independent form), eventually coupled to a time-dependent description of the kinetics of heavy-species, namely if the time-scales considered are above ~ 100 μs. Work is in progress to upgrade LoKI-B with

a time-dependent algorithm for monitoring the temporal evolution of the EEDF.

5. Final remarks

This topical review presented LoKI-B, a flexible and upgradable open-source simulation tool (`https://github.com/IST-Lisbon/LoKI`), licensed under the *GNU general public license*, for studying the non-equilibrium electron kinetics of LTPs excited by DC/HF electric fields. LoKI-B solves a time and space independent form of the EBE, written in the classical two-term approximation and including first-kind, second-kind and electron-electron collisions, assuming either a space-homogeneous exponential temporal growth or a time-constant exponential spatial growth of the electron density, to account for variations in the number of electrons due to non-conservative events. The tool simulates plasmas produced from different gases or gas mixtures, accounting for the internal distributions of populations for the electronic, vibrational and rotational atomic / molecular levels present in the plasma. On output, LoKI-B yields the EEDF, the electron swarm parameters, and the electron power absorbed from the electric field and transferred to the different collisional channels. The latter parameters can be calculated using either the distribution function obtained from the solution to the EBE or some other form prescribed by the user. As part of its development road-map, the tool has been checked in some test-cases, comprising the verification against analytical results, the benchmarking against numerical calculations obtained with BOLSIG+, and the validation by comparison with available measurements of swarm parameters.

LoKI-B is freely available for users to perform electron kinetics calculations, and for modellers who are invited to continue testing the tool and/or to contribute for its development and improvement. As any numerical tool, LoKI-B provides a mere representation of the energy distribution of the electrons in a LTP, because it is based on a specific formulation with embedded approximations. Therefore, the tool should be used only in situations fitting its validity limits, and users are advised to check section 3.6 and to carefully read the extensive literature on the two-term EBE [1], for obtaining details about its solution. The ontology of LoKI-B separates the tool and the data, but good use of the tool is naturally associated with the choice of adequate input cross sections and the definition of a proper energy-grid. As general guidelines, the preference should be for *complete sets* of cross sections (cf. section 3.3), giving a good description of all the electron energy and momentum losses, and a numerical grid with maximum energy below the cutoff energies of the cross sections and an energy step able to resolve any relevant structure in the data (e.g near-threshold variation, resonances, ...). Again, users are responsible for the correct choice of the input cross sections (obtained or not from LXCat) and the numerical grid, which must be carefully validated / evaluated according to the specific needs and the conditions of interest for the simulations.

LoKI-B is developed with object-oriented programming under MATLAB®, meaning that it can benefit from all the features associated with this platform. In particular, future developments of the tool could include a variety of capabilities, promoting its

integration with other codes and/or the exchange of data, such as [37]: parallel and/or cloud computing, web deployment and embedded code generation.

The future evolution of LoKI-B will include the adoption of a time-dependent algorithm to monitor the temporal evolution of the EEDF; and the extension of the formulation to obtain both the transverse and the longitudinal electron diffusion coefficients, and to simulate also weakly-magnetised LTPs. These and other developments will be always followed by V&V procedures, to ensure the quality of the tool and the output.

Acknowledgments

This work was funded by Portuguese FCT - Fundação para a Ciência e a Tecnologia, under projects UID/FIS/50010/2013 and PTDC/FISPLA/1243/2014 (KIT-PLASMEBA).

References

[1] Alves L L, Bogaerts A, Guerra V and Turner M M 2018 *Plasma Sources Sci. Technol.* **27** 023002

[2] This is not an extensively list, and the authors apologize if some relevant contributions were not highlighted here

[3] Frost L S and PheIps A V 1962 *Phys. Rev.* **127** 1621-1633

[4] Engelhardt A G and Phelps A V 1963 *Phys. Rev.* **131** 2115-2138

[5] Newman L A and DeTemple T A 1976 *J. Appl. Phys.* **47** 1912-1915

[6] Taniguchi T, Tagashira H and Sakai Y 1978 *J. Phys. D: Appl. Phys.* **11** 1757-1768

[7] Nighan W L 1970 *Phys. Rev.* A **2** 1989-2000

[8] Morgan W L 1979 *JILA Information Center Report* No. 19 (Univ. of Colorado, CO)

[9] Rockwood S D 1973 *Phys. Rev.* A **8** 2348-2358

[10] Rockwood S D 1974 *J. Appl. Phys.* **45** 5229-5234

[11] Rockwood S D and Greene A E 1980 *Comp. Phys. Comm.* **19** 377-393

[12] Winkler R B, Wilhelm J and Winkler R 1982 *Beitr. Plasma Phys.* **22** 401-413

[13] Elliott C J and Greene A E 1976 *J. Appl. Phys.* **47** 2946-2953

[14] Bretagne J, Godart J and Puech V 1982 *J. Phys. D: Appl. Phys.* **15** 2205-2226

[15] Capitelli M, Dilonardo M and Gorse C 1979 *Chem. Phys.* **43** 403-414

[16] Capitelli M, Dilonardo M and Gorse C 1981 *Chem. Phys.* **56** 29-42

[17] Loureiro J and Ferreira C M 1986 *J. Phys. D: Appl. Phys.* **19** 17-36

[18] Pitchford L C, O'Neil S V and Rumble Jr J R 1981 *Phys. Rev.* A **23** 294-304

[19] Pitchford L C and Phelps A V 1982 *Phys. Rev.* A **25** 540-554

[20] Yoshida S, Phelps A V and Pitchford L C 1983 *Phys. Rev.* A **27** 2858-2867

[21] Capitelli M, Gorse C, Wilhelm J and Winkler R 1981 *Lett. Nuovo Cimento* **32** 225-230

[22] Gorse C, Capitelli M and Dipace A 1990 *J. Appl. Phys.* **67** 1118-1120

[23] Winkler R, Braglia G L and Wilhelm J 1995 *Contrib. Plasma. Phys.* **35** 179-193

[24] Maeda K and Makabe T 1994 *Jpn. J. Appl. Phys.* **33** 4173-4176

[25] Morgan W L and Penetrante B M 1990 *Computer Physics Communications* **58** 127-152

[26] `http://kinema.com/elendif/` (last access January 29, 2019)

[27] `https://www.bolsig.laplace.univ-tlse.fr/` (last access January 29, 2019)

[28] Hagelaar G J M and Pitchford L C 2005 *Plasma Sources Sci. Technol.* **14** 722–733

[29] Dyatko N A, Kochetov I V, Napartovich A P and Sukharev A G 2015 *EEDF: the software package for calculations of the electron energy distribution function in gas mixtures*, `http://www.lxcat.net/software/EEDF/` (last access January 29, 2019)

[30] `https://github.com/aluque/bolos` (last access January 29, 2019)

[31] `www.lxcat.net/download/METHES` (last access January 29, 2019)

[32] Rabie M and Franck C M 2016 *Comput. Phys. Comm.* **203** 268-277

[33] `http://magboltz.web.cern.ch/magboltz/` (last access January 29, 2019)

[34] Biagi S F 1999 *Nuclear Instruments and Methods in Physics Research A* **421** 234-240

[35] https://gitlab.com/LXCatThirdParty/MultiBolt

[36] Stephens J 2018 *J. Phys. D: Appl. Phys.* **51** 125203

[37] `https://www.mathworks.com/products/matlab.html` (last access January 29, 2019)

[38] `www.lxcat.net` (last access January 29, 2019)

[39] Allis W P 1956 Motions of ions and electrons *Handbuck der Physik ed S Flugge* vol 21 (Berlin: Springer) pp 383–444

[40] Lorentz H A 1905 The motion of electrons in metallic bodies I *Proc. Royal Netherlands Academy of Arts and Sciences (KNAW)* vol 7 (Amsterdam: KNAW) pp 438–53

[41] Stephens J 2018 *Physics of Plasmas* **25** 103502

[42] Samukawa S, Hori M, Rauf S, Tachibana K, Bruggeman P, Kroesen G, Whitehead J C, Murphy A B, Gutsol A F, Starikovskaia S, Kortshagen U, Boeuf J P, Sommerer T J, Kushner M J, Czarnetzki U and Mason N 2012 *J. Phys. D: Appl. Phys.* **45** 253001

[43] Reid I D 1979 *Aust. J. Phys.* **32** 231-254

[44] Chantry P J, Phelps A V and Schulz G J 1966 *Phys. Rev.* **152** 81-98

[45] Lucas J and Salee H T 1975 *J. Phys. D: Appl. Phys.* **8** 640-650

[46] Ness K F and Robson R E 1986 *Phys. Rev.* A **34** 2185-2209

[47] Petrović Z Lj, Dujko S, Marić D, Malović G, Nikitović Ž, Šašić O, Jovanović J, Stojanović V and Radmilović-Radenović M 2009 *J. Phys. D: Appl. Phys.* **42** 194002

[48] Pack J L, Voshall R E and Phelps A V 1962 *Phys. Rev.* **127** 2084-2089

[49] Crompton R W 1994 *Adv. At. Mol. Opt. Phys.* **33** 97-148

[50] Huxley L G H and Crompton R W 1974 *The Diffusion and Drift of Electrons in Gases* (New York: Wiley-Interscience)

[51] Hunter S R and Christophorou L G 1984 *Electron Molecule Interactions and their Applications* vol 2, ed L G Christophorou (New York: Academic)

[52] Morgan W L 2000 *Adv. At. Mol. Opt. Phys.* **43** 79-110

[53] Petrović Z Lj, Suvakov M, Nikitović Ž, Dujko S, Šašić O, Jovanović J, Malović G and Stojanović V 2007 *Plasma Sources Sci. Technol.* **16** S1-S12

[54] White R D, Ness K F and Robson R E 2002 *Appl. Surf. Sci.* **192** 26-49

[55] Turner M, *Plasma Process. Polym.* 2017 **14** 1600121

[56] Pitchford L *et al* 2017 *Proc. 70*th *Gaseous Electronics Conference* (GEC), Pittsburgh, USA in *Bull. Am. Phys. Soc.* **62** 10

[57] Ridenti M A, Alves L L, Guerra V and Amorim J 2015 *Plasma Sources Sci. Technol.* **24** 035002

[58] `https://www.ipfn.tecnico.ulisboa.pt/nprime/` (last access January 29, 2019)

[59] KInetic Testbed for PLASMa Environmental and Biological Applications (KIT-PLASMEBA), `http://plasmakit.tecnico.ulisboa.pt/` (last access January 29, 2019)

[60] Guerra V and Loureiro J 1997 *Plasma Sources Sci. Technol.* **6** 373-385

[61] Alves L L 2007 *Plasma Sources Sci. Technol.* **16** 557-569

[62] Šimek M and Bonaventura Z 2018 *J. Phys. D: Appl. Phys.* **51** 504004

[63] Holstein T 1946 *Phys. Rev.* **70** 367–84

[64] Delcroix J-L 1963/1966 *Physique des Plasmas* (*Monographies Dunod* vol 1 et 2) (Paris: Dunod) (in French)

[65] Tagashira H, Sakai Y and Sakamoto S 1977 *J. Phys. D: Appl. Phys.* **10** 1051-1064

[66] Thomas W R L 1969 *J. Phys. B: At. Mol. Phys.* **2** 551-561

[67] Chapman S and Cowling T G 1939 *The Mathematical Theory of Non-uniform Gases* (Cambridge: Cambridge University Press)

[68] Shkarofsky I, Johnston T and Bachynski M 1966 *The Particle Kinetics of Plasmas* (Addison-Wesley Publishing Company)

[69] Dyatko N A, Kochetov I V and Napartovich A P 1993 *J. Phys. D: Appl. Phys.* **26** 418-423

[70] Ferreira C M and Loureiro J 2000 *Plasma Sources Sci. Technol.* **9** 528-540

[71] Klein O and Rosseland S 1921 *Z. Phys.* **4** 46-51

[72] Pitchford L C, Alves L L, Bartschat K, Biagi S F, Bordage M C, Phelps A V, Ferreira C M, Hagelaar G J M, Morgan W L, Pancheshnyi S, Puech V, Stauffer A and Zatsarinny O 2013 *J. Phys. D: Appl. Phys.* **46** 334001

[73] Opal C, Peterson W and Beaty E 1971 *J. Chem. Phys.* **55** 4100–4106

[74] Kim Y-K 1995 *Atomic and Molecular Processes in Fusion Edge Plasmas* (Springer Science, Business Media, New York)

[75] Rudd M E 1991 *Phys. Rev.* A **44** 1644-1652

[76] Alves L L 2014 *J. Phys. Conf. Series* **565** 012007

[77] Alves L L, Marques L, Pintassilgo C D, Wattieaux G, Es-sebbar Et, Berndt J, Kovačević E, Carrasco N, Boufendi L and Cernogora G 2012 *Plasma Sources Sci. Technol.* **21** 045008

[78] Turner M M 2015 *Plasma Sources Sci. Technol.* **24** 035027

[79] Amemiya H 1997 *J. Phys. Soc. Jpn.* **66** 1335-1338

[80] Nama S K and Verboncoeur J P 2009 *Computer Physics Communications* **180** 628–635

[81] Toneli D A, Pessoa R S, Roberto M and Gudmundsson J T 2015 *J. Phys. D: Appl. Phys.* **48** 495203
[82] Margenau H 1946 *Phys. Rev.* **69** 508–513
[83] `Ar` on IST-Lisbon database, `www.lxcat.net`, retrieved on June 2018
[84] `Ar` on Dutton database, `www.lxcat.net`, retrieved on June 2018
[85] `Ar` on LAPLACE database, `www.lxcat.net`, retrieved on June 2018
[86] Nielsen R A 1936 *Phys. Rev.* **50** 950–954
[87] Bowe J C 1960 *Phys. Rev.* **117** 1411–1415
[88] Pack J L and Phelps A V 1961 *Phys. Rev.* **121** 798–806
[89] Wagner E B, Davis F J and Hurst G S 1967 *J. Chem. Phys.* **47** 3138–3147
[90] Robertson A 1977 *Aust. J. Phys.* **30** 39-50
[91] Christophorou L G, McCorkle D L, Maxey D V and Carter J G 1979 *Nucl. Instruments Methods* **163** 141–149
[92] Nakamura Y and Kurachi M 1988 *J. Phys. D: Appl. Phys.* **21** 718–723
[93] Kucukarpaci H N and Lucas J 2001 *J. Phys. D: Appl. Phys.* **14** 2001–2014
[94] Lakshminarasimha C S and Lucas J 1977 *J. Phys. D: Appl. Phys.* **10** 313–321
[95] Milloy H B and Crompton R W 1977 *Aust. J. Phys.* **30** 51-60
[96] Al-Amin S A J and Lucas J 1987 *J. Phys. D: Appl. Phys.* **20** 1590–1595
[97] Townsend J S and Bailey V A 1922 *Philos. Mag. J. Sci.* **44** 1033–1052
[98] Warren R W and Parker J H 1962 *Phys. Rev.* **128** 2661–2671
[99] Kruithof A A and Penning F M 1936 *Physica* **3** 515-533
[100] Kruithof A A 1940 *Physica* **7** 519-540
[101] Golden D E and Fisher L H 1961 *Phys. Rev.* **123** 1079-1086
[102] Specht L T, Lawton S A and De Temple T A 1980 *J. Appl. Phys.* **51** 166-170
[103] Puech V and Torchin L 1986 *J. Phys. D: Appl. Phys.* **19** 2309-2324
[104] Jelenak Z M, Velikić Z B, Božin J V, Petrović Z Lj and Jelenković B M 1993 *Phys. Rev.* E **47** 3566-3573
[105] Božin J V, Jelenak Z M, Velikić Z V, Belča I D, Petrović Z Lj and Jelenković B M 1996 *Phys. Rev.* E **53** 4007-4011
[106] `N2` on IST-Lisbon database, `www.lxcat.net`, retrieved on June 2018
[107] Frommhold L 1960 *Z. Physik* **160** 554-567
[108] Wagner K H and Raether H 1962 *Z. Physik* **170** 540-544
[109] Lowke J J 1963 *Australian J. Phys.* **16** 115-135
[110] Engelhardt A G, Phelps A V and Risk C G 1964 *Phys. Rev.* A **135** 1566-1574
[111] `Air` on LAPLACE database, `www.lxcat.net`, retrieved on June 2018
[112] `Air` on Dutton database, `www.lxcat.net`, retrieved on June 2018
[113] Frommhold L 1964 *Fortschr. Physik* **12** 597-642
[114] Hessenauer H 1967 *Z. Physik* **204** 142-154
[115] Nielsen R A and Bradbury N E 1937 *Phys. Rev.* **51** 69-75
[116] Ryzko H 1965 *Proc. Phys. Soc. London* **85** 1283-1296
[117] Rees J A 1973 *Aust. J. Phys.* **26** 427-432
[118] Roznerski W and Leja K 1984 *J. Phys. D: Appl. Phys.* **17** 279-286
[119] `O2` on IST-Lisbon database, `www.lxcat.net`, retrieved on June 2018
[120] Treanor C E, Rich J W and Rehm R G 1968 *J. Chem. Phys.* **48** 1798-1807
[121] Gordiets B, Mamedov Sh. and Shelepin L 1975 *Sov. Phys. - JETP* **40** 640-646
[122] Annušová A, Marinov D, Booth J-P, Sirse N, Lino da Silva M, Lopez B and Guerra V 2018 *Plasma Sources Sci. Technol.* **27** 045006
[123] Marinov D, Foucher M, Guaitella O, Engeln R, Laux C, Chabert P, Guerra V and Booth J-P 2016 *Proceedings XXIII Europhysics Conference on Atomic and Molecular Physics of Ionized Gases* (ESCAMPIG), p. 295, Bratislava, Slovakia
[124] Annušová A, Guerra V, Lino da Silva M, Lopez B, Foucher M, Marinov D and Booth J-P 2016

Proceedings XXIII Europhysics Conference on Atomic and Molecular Physics of Ionized Gases (ESCAMPIG), p. 333, Bratislava, Slovakia

[125] Booth J-P, Foucher M, Marinov D, Gibson A, Chabert P, Annušová A and Guerra V 2016 *Proceedings XXIII Europhysics Conference on Atomic and Molecular Physics of Ionized Gases* (ESCAMPIG), p. 385, Bratislava, Slovakia

[126] Snoeckx R, Aerts R, Tu X and Bogaerts A 2013 *J. Phys. Chem. C* **117** 4957-4970

[127] Kozák T and Bogaerts A 2014 *Plasma Sources Sci. Technol.* **23** 045004

[128] Koelman P, Heijkers S, Mousavi S T, Graef W, Mihailova D, Kozak T, Bogaerts A and van Dijk J 2017 *Plasma Process Polym* **14** 1600155

[129] Luo Y, Lietz A M, Yatom S, Kushner M J and Bruggeman P J 2019 *J. Phys. D: Appl. Phys.* **52** 044003